ABSTRACT

Title of Document: NONFARADAIC IMPEDIMETRIC SENSING OF BIOMOLECULES ON GOLD ELECTRODES FOR APPLICATIONS IN LABEL-FREE BIOSENSORS

Yusmeeraz Binti Yusof

Supervised By: Professor Kazuo Nakazato,
Graduate School of Engineering, Nagoya University

Biosensors have emerged as a key tool for point-of-care (POC) diagnostics that allows the patient or physicians to get results quickly and easily on site due to their inherent small size and simple instrumentation. Glucose biosensors are the most common POC devices commercially available and a well-known example is the Abbott i-STAT® handheld blood analyzer, which is capable of performing a panel of frequently ordered blood tests on two or three drops of blood at the patient's side. Recently, molecular analysis focused on the detection of nucleotides (i.e. DNA) is finding increasing attention as it can serve as early indicators of fatal disease such as cancer and greatly improves the chances of a cure. Biosensors based on electrochemical reactions can directly generate an electronic signal and operate in label-free, provides a simple and low-cost approach over conventional method that rely on a label or redox-active signal from a reporter molecules. Label-free electrochemical biosensors may be subdivided into potentiometric, amperometric, or impedimetric types. Since any piece of human body, such as DNA, proteins, and cells have their unique impedance values, impedance-based measurement appears as a well suited and powerful technique for biomolecular sensing. In addition, nonfaradaic impedimetric biosensor offers the simplest structure and most direct signal transduction without the use of any redox indicator that reduce the cost of fabrication and enhance the reliability of test results, that is, more amenable to POC applications. This thesis work is inserted in this field. Sensing principle relies on changes in electrical double layer properties of the biomodified electrode surface is exploited to achieve a fully label-free DNA detection. The feasibility of using an on-chip gold microelectrode with complimentary metal oxide semiconductor (CMOS) detection circuit is proposed and demonstrated. Charge-based capacitance measurement (CBCM) technique is employed to detect the interface capacitance changes as a result of biomodification or birecognition event at electrode surface. In order to eliminate variations in the sensed signal caused by uncontrolled disturbances such as salt concentration, pH or temperature, fully differential scheme is applied at the circuitry design and the output current of CBCM is directly

translated into voltage using a current-to-voltage converter. Linear sensitivity of 3 mV/fF for the input range of 1 to 10^3 fF is achieved in a 1.2 μm CMOS technology. Sensing electrode is fabricated through the use of via in standard chip fabrication process and patterned in-house using conventional lithography after thermal evaporation of titanium and gold. The circuit is characterized using various sodium chloride solutions and the results show that the capacitance increases as the solution concentration increases as expected. It is found that this capacitance is a frequency dependent. DNA detection is demonstrated by monitoring the changes before and after DNA hybridization in a phosphate buffer solution. A capacitance change of about 20% (10 fF) over a wide frequency is observed after exposing of surface-tethered single-stranded DNAs to its complementary strands, which implies that the physical properties of the double layer are altered upon the hybridization. Biochemical phenomena underlying this capacitance variation is further investigated using electrochemical impedance spectroscopy measurement. For this purpose, two-electrode liquid test fixture that is specially-made with built-in and disposable gold electrode features is employed in conjunction with an impedance analyzer. From the results, it is found that the interface impedance is best represented by a constant phase element and can be modeled by a parallel combination of a high-resistance parameter and a capacitive parameter. To observe the interfacial property change induced by electrical double layer variation, a measurement using self-assembled monolayer of mercaptohexanol (MCH) is performed. A significant decrease in capacitance and increase in resistance are observed upon MCH modification. Since the monolayer is assumed to act as an insulator and thus push the electrolyte ions far from the electrode, the above observation suggests that the decrease in capacitance and increase in resistance are due to the increase in electrical double layer thickness and reduction in accessibility of ions to the surface of gold electrode, respectively. Later, the detection of complementary DNA hybridization is demonstrated. Two types of probe-tethered surface without and with MCH backfilling are prepared. MCH is used to fill any defects of the DNA monolayer formed on the gold surface. The Nyquist plots clearly distinguish the impedance of electrode between before hybridization and after hybridization, particularly at low frequency region below 1 kHz. It is found that this impedance change is probably due to the physical changes of DNA molecules that results in the variation of electrical double layer thickness. A decrease in resistance after hybridization suggests that the transformation of a flexible single-stranded DNA into a rigid double-stranded DNA might cause an opening space at the interface, allowing the electrolyte ions to get closer to the electrode. It is believed that the resulted capacitance change or more specifically, the effective double layer thickness is dependent on this behavior. These findings will hopefully provide a basis for a better fundamental understanding of the associated impedance changes due to DNA hybridization and may help in guiding the development of low cost, yet reliable fully integrated genomic assays for point-of-care use.

Acknowledgment

First I am very grateful to my supervisor, Professor Nakazato, for the opportunity to work in his laboratory at Nagoya University. I appreciate for his guidance, advice, patience and understanding on my research work and even on personal issues.

I would also like to thank the dissertation committee members, Prof. Iwata, Prof. Amano, Assoc. Prof. Uchiyama, and Dr. Kamahori (Central Research Laboratory, Hitachi Ltd., Tokyo) for their time and effort to evaluate and improve my dissertation. I wish to express my sincere thanks to Mr. Yoshiyuki Yanagimoto (Agilent Technologies International Japan Ltd., Kobe) for his support and valuable research discussion in impedance measurement.

I am very fortunate to have the opportunity to work with many amazing people at Nakazato Laboratory. Special thanks go to Asst. Prof. Shigeyasu Uno, a former colleague, for his inspiring and motivating encouragements as well as constructive criticism are vital to my professional and personal development. I am also indebted to my former group members Kiyomasa Sugimoto and Park Guijin for their important contributions to this research. I thank my former colleagues Dr. Hiroaki Ozawa for teaching me biological chemistry and Ms. Mio Ishihama for her help and guidance in chip post-processing. I would also like to extend my gratitude to all the past and present laboratory members, especially J. Hattori, B. Kim, T. Numata, M. Iio, J. Hasegawa, and H. Matsumoto, with whom I spent the longest time worked together. My graduate study experience would not have been as wonderful without them.

I dearly thank my husband, Emran for believing in me and my family for their love and unconditional support during my study years.

Finally, I wish to acknowledge the Malaysian Government Scholarship Program under SLAB Grant and the Universiti Teknologi Malaysia for their financial support.

List of contents

Chapter 1

Introduction

1.1 Background and motivation

Identification of human genome using nucleic acid assays is extremely important for diagnosis and personalized treatments of genetic-related diseases. Genetic diseases are not restricted to those inherited from parents to offspring [1], but also those whose root-cause is genetic in nature, such as cancers, Down syndrome, and diabetes. Many of these genetic disorders are caused by small changes or mutations of deoxyribonucleic acid (DNA), the hereditary material of all living cells that comprises the blueprint of individual genetic profile. The availability of DNA data could help to screen gene abnormalities and provide valuable medical information for early detection of fatal diseases that implies a better chance for a cure with more treatment options. Hence the recognition or detection of DNA sequence is vital in the diagnosis of genetic-related diseases. One conventional way to detect DNA is by the use of affinity binding or hybridization of single-stranded DNA (referred to as a 'probe') to its complementary sequence (referred to as a 'target') to form a stable double-stranded DNA [2, 3]. To date, detection method has relied on labeling of DNA samples followed by optical readout, a process which can be time-consuming, labor-intensive and expensive. Although label-based DNA detection have been shown to achieve very high sensitivity of picomolar (pM) range with very sophisticated photomultiplier detectors [4], the instruments are oftentimes bulky and not easy-handling, thus inhibited the widespread use outside the sophisticated research laboratories. Recently, a low-cost and portable device that could be used in a point-of-care (POC) environment for rapid DNA diagnosis is strongly demanded [5]. POC testing has drastically revolutionized medical diagnostics by enabling physicians to do such a testing at or near the site of patient care. It provides immediate information about the patient's condition, so that physicians can make the appropriate treatment decisions in case of an emergency, resulting in improvements in patient criticality and mortality. POC tests are also convenient as part of daily routine medical checkups for prevention or monitoring of fatal disease. In that regard, electrical DNA biosensors are

one strategy being explored for the development of POC tools since this technology is amenable to miniaturization, can be accurate and sensitive with simple instrumentation, and relatively inexpensive. Therefore, this thesis work is focused on developing a DNA assay using electrical detection scheme that would meet the requirements of POC diagnostics. The main goal is to lay the groundwork for establishing the feasibility of a nonfaradaic impedimetric based system, a method that is fully label-free by only relying on changes in the electric properties of the DNA modified interface at sensing electrode. Instead of a conventional three-electrode system, a simple two-electrode structure for capacitive sensing is employed in this work so that the need of reference electrode can be eliminated. Thus, compared to other label-free detection methods including amperometric or potentiometric where reference electrode is a must, it is considered that the proposed approach is advantageous in terms of cost and simplicity for future integration.

This thesis starts with the following subchapter by introducing the brief explanation of DNA and its application in gene analysis. Chapter 2 is the review of other viable DNA detection schemes to show that the proposed method is worth the pursuit. Chapter 3 describes a proposed system for on-chip DNA detection using charge-based capacitance measurement (CBCM). Sensing principle that exploits the electrical double-layer changes as a result of biomodification or biorecognition event and chip architecture employing standard complimentary metal oxide semiconductor (CMOS) technology are presented. Later, the feasibility of the fabricated chip is examined using sodium chloride solution and DNA detection using 20-mer oligonucleotides hybridization is demonstrated. This thesis also describes an investigation of underlying biochemical phenomena during DNA modification that caused the variation of the interfacial layer. Chapter 4 is related to electrochemical impedance spectroscopy (EIS) study of the interfacial region. Electrical characteristics of the modified electrodes are estimated using an equivalent circuit model that is deduced from the complex impedance data. Impedance change upon biomodification of self-assembled monolayer (SAM) of mercaptohexanol (MCH) and hybridization of complementary DNA using two surfaces of probe DNA without and with MCH backfilling are investigated. All measurements are performed with a specially-made two-electrode liquid test fixture with an impedance analyzer in an electrolyte solution. Finally, conclusions are given and future work is also discussed.

1.2 Deoxyribonucleic acid

Deoxyribonucleic acid (DNA) was first identified in 1869 by Swiss chemist Johann Friedrich Miescher [6]. DNA is composed of a series of nucleotides and that each nucleotide has three components: a phosphate group, a deoxyribose sugar, and a single nitrogen-containing base. There are two basic categories of nitrogenous bases: the purines (adenine (A) and guanine G)), each with two fused rings; and the pyrimidines (cytosine (C) and thymine (T)), each with a single ring (Fig. 1.1). In 1950, Erwin Chargaff, an Austrian biochemist, found that in DNA, the content of purines (adenines + guanines) was always roughly equal to the content of pyrimidines (cytosines + thymines). Furthermore, the amounts of adenine and thymine were roughly equal, so were the amounts of guanine and cytosine. This was known as Chargaff's rule [1]. The nucleotides are covalently joined through 3', 5'- phosphodiester bonds thus forming a single DNA strand (Fig. 1.2). The order of the bases in a DNA strand plays a vital role in living cells, because the base sequence encodes the genetic information.

1.2.1 Double-helix DNA

In 1953, Francis Crick and James Watson proposed that the DNA molecule has a double-helical structure. As depicted in Fig. 1.3, DNA is a double-stranded helix, with the two single DNA strands comprised of the sugar-phosphate backbone and the alternating bases are connected by hydrogen bonds. The DNA double helix is anti-parallel, which means that the 5' end of the strand is paired with the 3' end of the other strand (and vice versa) [7]. The bases must be paired with a purine in one side and a pyrimidine in the other side. Watson and Crick postulated from Chargaff's rule that adenines must always bind with thymines by means of two hydrogen bonds, and guanines must always bind with cytosines by means of three hydrogen bonds. This complementary bases form is known as Watson-Crick base pairing (A-T, C-G) and is the basis of two molecular mechanisms; replication and recognition. The former is the process by which a double-stranded DNA is separated, and each can then serve as a copy template to produce two identical DNA molecules. Replication is an essential process because whenever a cell divides, the two new daughter cells must contain the same genetic information as the parent cell, preserving the genes or DNA as the cells divide. The

latter based on the affinity reaction so-called hybridization of one single strand to form a double-helix with another single strand of complementary base sequence as they can recognize specifically each other. This has been the key principle for several recombinant nucleic acid techniques such as genotyping, fingerprinting and mutation analysis (also known as Single Nucleotide Polymorphism analysis) that are capable to identify DNA. Detection of DNA allows the searching of DNA change and sequence abnormalities that can flags a marker of certain diseases or a reaction to drugs. There are at least 400 diseases that can be diagnosed through the identification of genes with the help of DNA assays [8]. It also finds forensic uses, for instance, identity testing as DNA fingerprint (i.e. the repeat pattern of sequences of bases) is unique for every individual.

1.2.2 DNA analysis technologies: Microarray and biosensor

Current genomic technologies that involve sequence recognition by hybridization are microarrays and biosensors. In these technologies, a surface-tethered single strand with known sequence (referred to as a probe DNA) is used to capture its corresponding complementary strand present in an analyte solution, whose sequence is to discover (referred to as a target DNA). Physical or chemical changes upon the occurrence of hybridization are then detected and interpreted by a slew of methods.

In a DNA microarray, probe DNAs are spotted and chemically or physically attached onto a glass substrate. Each DNA spot in the microarray contains one specific sequence corresponding to a specific gene, thus thousands of genes are able to search in one experiment by parallel readout. The most common way in microarray is to label the target DNAs with fluorescent dye, and to hybridize the analyte solution to the microarray-attached probe DNAs. Owing to Watson-Crick base pairing rules, certain genes in the analyte will selectively bind to its matching probe on the microarray. After washing to remove excess and non-specific binding, the microarray is scanned by the use of a laser scanner for the fluorescent signals emitted by the hybridized spot. Since the sequence on each spot in the array is known, one can straightforwardly identify what genes contained in the unknown analyte by looking at which spots fluoresce. Microarray can also be used to do comparative assay of DNA (see Fig. 1.4). Two DNA samples are extracted from normal cells of a healthy person and tumor cells from a patient. The samples are labeled with two different dyes. Normal cells are often labeled with green fluorescent dyes, and tumor cells are labeled with red. The two samples are then mixed

together and hybridized to a single DNA microarray. The target genes from the two cells would compete for the same probe DNA. The microarray is then scanned in a sophisticated scanner to visualize fluorescence after excitation with a laser beam. By comparing the relative color intensities, i.e. greenish or reddish, ratio-based analysis can be done. If the spot appears red, the tumor cells have expressed more of the genes in that corresponding spot than the normal cells. If the spot appears yellowish, then both normal and tumor cells have very similar expression levels. The sensitivity of microarray has been claimed to go down to picomolar [4] and even to 3 zeptomolar if using signal amplification [9]. One of the most successful microarray developers is Affymetrix, Inc. Instead of robotic spotting, the probe DNAs or spots on a Affymetrix chip, so-called GeneChip® are built-up one nucleotide at a time using a unique photolithographic process. Each spot size is only several microns to make a very dense array that corresponds to an array density of 10^6 probes cm^{-2}, as opposed to several hundred microns in robotic spotted microarray. Despite the ability to achieve high sensitivity and high throughput analysis using microarray technologies, main drawbacks are the laborious protocol in sample preparation and labeling step that is time consuming and labor intensive, and requirement of expensive and large detection instrumentation. All these impediments limit its deployment in point-of-care environment.

Recently, biosensors emerge as alternative technologies by offering the possibility of low cost and miniaturization for development of a portable and affordable device for point-of-care diagnostics. In biosensor, the readout of the hybridization event occurs usually at a solid state to which a probe DNA acts as a biorecognition element is attached to the transducer surface. The target DNA in solution is selectively captured by a surface-tethered probe DNA and the electrochemical reaction that occurred is then translated into a detectable signal by a given transduction mechanism to be processed by a computer for its interpretation. The transduction mechanism can consist of changes in electrochemical properties (i.e. surface potential, redox kinetics, impedance, etc.) or changes in non-electrochemical properties (i.e. conformation changes, mass transportation, van der Waals interactions, etc.). The resultant signal readouts can take the form as electrical currents, potentials, or impedances in steady state or changes in these parameters during the recognition process [10, 11]. Biosensors can be divided into two categories: labeled detection and label-free detection. The first category, usually use labeled reporters, such as intercalators (which intercalate between stacked bases in double-stranded DNA) and redox tags (which covalently bound to the target or probe DNA).

Some commonly used reporters are methylene blue [12, 13], cobalt phenanthroline [14], and ferrocene [15, 16]. Usually label-free detection refers to detection that not requiring any label to be linked to the target or to the probe. The monitoring of hybridization event is performed based on either the electroactivity of DNA itself or physical properties of the hybridized DNA surface such as dielectric constant, negative charges from DNA phosphate backbone (when ionized in a solution), and weight. The former exploited the oxidation of nucleotide bases such as guanine through direct oxidation at ca. 1.07 V [17, 18], where oxidative current proportional to the number of guanine residues. This method is destructive since the reaction is irreversible, and thus precludes the reuse of the same surface [19]. The latter exploited the changes in dielectric, mass or electrical properties of metal-electrolyte interface as an indicator of the hybridization event. The label-free schemes of this category will be reviewed in detail at the following chapter as this is the focus of this thesis, which are further divided into two groups: non-electrochemical sensors and electrochemical sensors.

[**References**]

1. R. F. Weaver, *Molecular biology.* 3rd ed. McGraw-Hill, 2004.
2. A. Chakravarti, *Population genetics-making sense out of sequence.* Nature genetics, 1999, 21 (1), pp. 56-60.
3. P. Y. Kwok, *Methods for genotyping single nucleotide polymorphisms*. Annu. Rev. Genomics Hum. Genet., 2001, 2, pp. 235-258.
4. I. Rech, S. Cova, A. Restelli, M. Ghioni, M. Chiari, M. Cretich, *Microchips and single-photon avalanche diodes for DNA separation with high sensitivity.* Electrophoresis, 2006, 27 (19), pp. 3797-3804.
5. J. Wang, *Electrochemical biosensors: Towards point-of-care cancer diagnostics.* Biosens. Bioelectron., 2006, 21 (10), pp. 1887-1892.
6. R. Dahm, *Friedrich Miescher and the discovery of DNA.* Developmental Biology, 2005, 278, pp. 274-288.
7. L. Pray, *Discovery of DNA structure and function: Watson and Crick*. Nature Education, 2008, 1 (1).
8. A. W. Peterson, L. K. Wolf, R. M. Georgiadis, *Hybridization of mismatched or partially*

matched DNA at surfaces. J. Am. Chem. Soc., 2002, 124 (49), pp. 14601-14607.

9. H. A. Ho, K. Dore, M. Boissinot, M. G. Bergeron, R. M. Tanguay, D. Boudreau, L. Leclerc, *Direct molecular detection of nucleic acids by fluorensence signal amplification.* J. Am. Chem. Soc., 2005, 127 (36), pp. 12673-12676.
10. F. Wei, P. B. Lillehoj, C. M. Ho, *DNA diagnostics: Nanotechnology-enhanced electrochemical detection of nucleic acids.* Pediatric Research, 2010, 67 (5), pp. 458-468.
11. A. J. Bard, L. R. Faulkner, *Electrochemical methods: Fundamentals and applications.* John Wiley & Sons, New York, 1980.
12. Y. Jin, X. Yao, Q. Liu, *Hairpin DNA probe based electrochemical biosensor using methylene blue as hybridization indicator.* Biosens. Bioelectron., 2007, 22 (6), pp. 1126-1130.
13. P. Kara, K. Kerman, D. Ozkan et al., *Label-free and label based electrochemical detection of hybridization by using methylene blue and peptide nucleic acid probes at chitosan modified carbon paste electrodes.* Electroanalysis, 2002, 14 (24), pp. 1685-1690.
14. K. M. Millan, S. R. Mikkelsen, *Sequence-selective biosensor for DNA-based on electroactive hybridization.* Anal. Chem., 1993, 65 (17), pp. 2317-2323.
15. C. Xu, H. Cai, P. G. He, Y. Z. Fang, *Elctrochemical detection of sequence-specific DNA using a DNA probe labeled with aminoferrocene and chitosan modified electrode immobilized with ssDNA.* Analyst, 2001, 126 (1), pp. 62-65.
16. H. Aoki, H. Tao, *Label- and marker-free gene detection based on hybridization-induced conformational flexibility changes in a ferrocene-PNA conjugate probe.* Analyst, 2007, 132, pp. 784-791.
17. E. Palecek, *Oscillographic polarography of highly polymerized deoxyribonucleic acid*. Nature, 1960, 188, pp. 656-657.
18. J. Wang, G. Rivas, J. R. Fernandes et al., *Indicator-free electrochemical DNA hybridization biosensor.* Anal. Chem. Acta, 1998, 375 (3), pp. 197-203.
19. J. Mbindyo, L. Zhou, Z. Zhang, J. D. Stuart, J. F. Rusling, *Detection of chemically induced DNA damage by derivative square wave voltammetry.* Anal. Chem., 2000, 72, pp. 2059-2065.

1.3 Figures

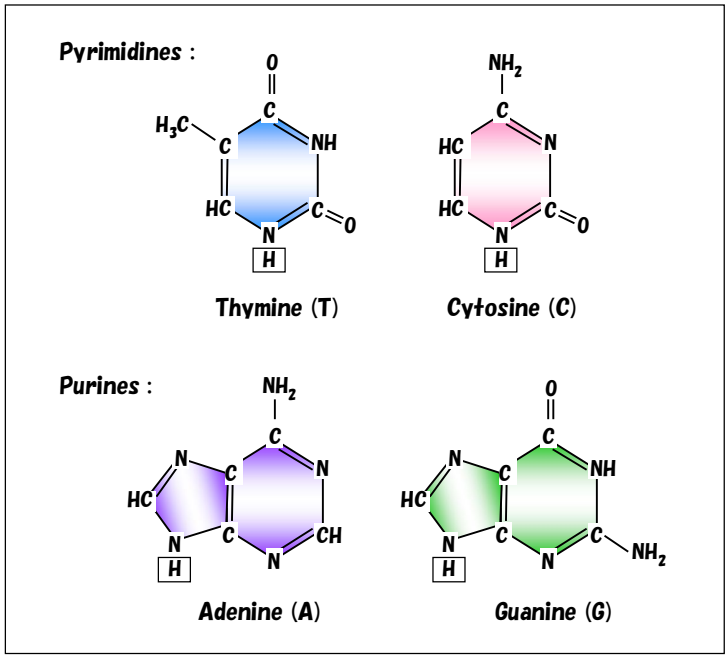

Fig. 1.1 A schematic of DNA bases: Adenine (A), Guanine (G), Cytosine (C), and Thymine (T).

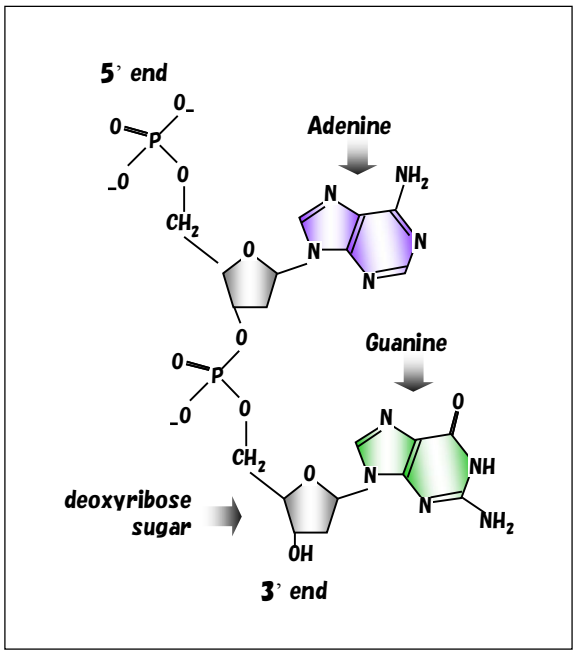

Fig. 1.2 A schematic view of a single strand DNA.

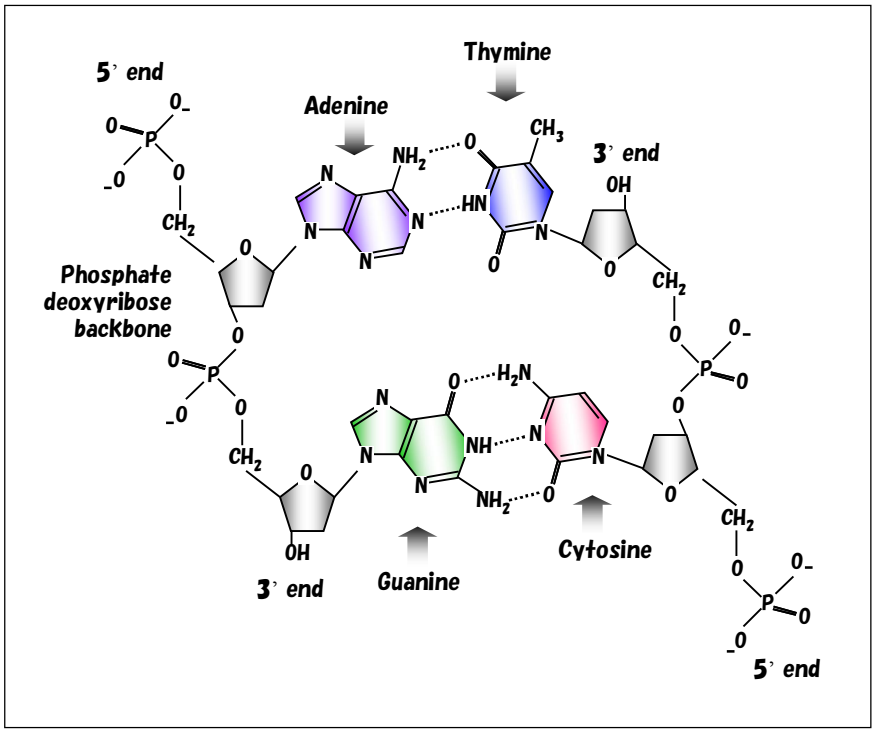

Fig. 1.3 Double-helix structure of DNA proposed by Crick and Watson.

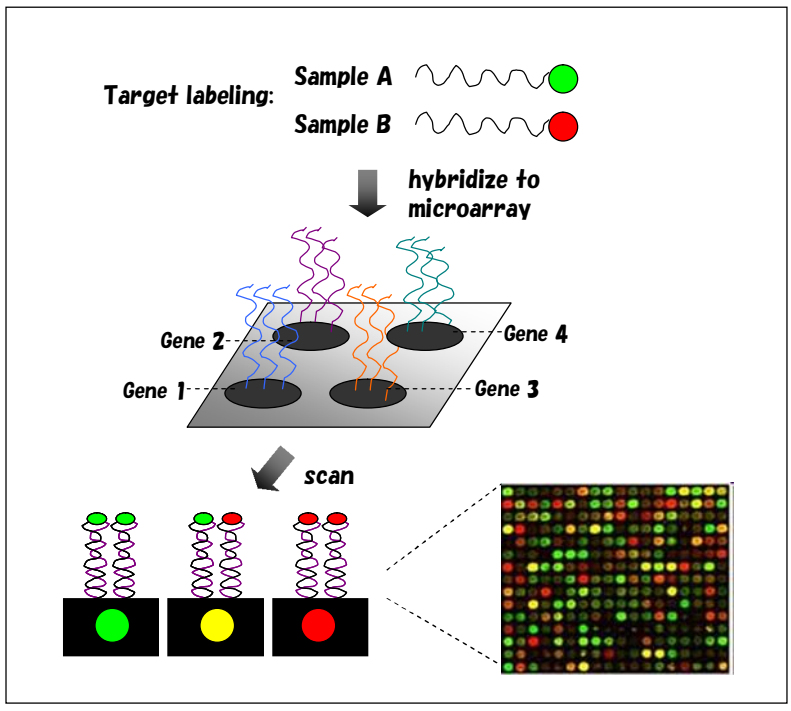

Fig. 1. 4 Comparative assay of DNA using microarray.

Chapter 2

Label-free DNA detection schemes

In this chapter, label-free DNA detection technologies that focused on physical properties changes at the electrode-solution interface are reviewed and classified based on the transduction mechanisms as follows: (1) non-electrochemical and (2) electrochemical.

2.1 Label-free (1): Non-electrochemical

Depending on the physical property changes that are sensed during DNA hybridization at the electrode surface, non-electrochemical biosensors can be divided into optical and gravimetric methods. Label-free optical method relies on dielectric property changes at the interface of a metal substrate and a DNA monolayer. Such is the case of surface plasmon resonance (SPR) [20]. It provides a non-invasive, label-free means of observing binding interactions between an analyte of target DNA and an immobilized probe DNA in real time. Gravimetric method tracks changes in mass on the surface of piezoelectric substrates that occur during DNA hybridization. An example is quartz crystal microbalance (QCM) where a change in the oscillation frequency of the sensor crystal is exploited to detect an adding or removing of DNA molecules on the sensor surface.

2.1.1 Surface plasmon resonance

SPR is a technique for detecting changes in refractive index on the surface of a sensor [21]. SPR transducers are usually constructed by using prism coupling of incident light onto an optical substrate that is coated with a semitransparent noble metal (e.g. gold) under conditions of total internal reflection. Light passes through the substrate and is reflected off of the gold coating (see Fig. 2.1). A condition of SPR will occur when the following conditions are satisfied. The incident wave vector is given by the following expression

$$K_i = \left(\frac{2\pi}{\lambda}\right) n \sin\theta_i \tag{1}$$

where K_i is a component of the incident light wave vector parallel to the prism interface, θ_i is the incident light angle, λ is the wavelength of the incident light and n is the refractive index of the prism. The wave vector of the plasmon mode is described by the following expression

$$K_p = \left(\frac{2\pi}{\lambda}\right)\sqrt{\frac{\varepsilon_1\varepsilon_2}{\varepsilon_1+\varepsilon_2}} \tag{2}$$

where K_p is the surface plasmon wave vector and ε_1 and ε_2 are the dielectric permittivity constants of the gold film and the dielectric exit medium, respectively. Surface plasmon resonance occurs when

$$K_i = K_p . \tag{3}$$

The intensity of the reflected light will decrease where SPR exists thereby giving rise to a well defined minimum in the reflectance intensity.

For biosensing, it is this change in the refractive index of the dielectric exit medium on the gold surface that is of interest. Therefore, if the refractive index of the prism is constant, then a change in the resonance condition may be related to changes in the refractive index of the exit medium. In this way, it is possible to monitor in real time the accumulation of biofilms on the gold surface in order to measure binding of biomolecules (i.e. DNA hybridization) to a surface that has been coated with an affinity ligand of probe DNA. Although SPR is very sensitive to tiny changes in refractive index, the refractive index of the analyte does not change much upon target binding because the refractive index of the buffer solution is already comparable to that of the target molecule. Moreover, the refractive index is also sensitive to temperature changes hence the temperature control of the instrument is essential for achieving a good sensitivity of SPR output. Nevertheless, direct assay detection of 10 nM target DNA oligonucleotide was achieved [22]. Currently, SPR sensors have been available commercially by vendors such as BIAcore AB (BIAcore®) and Nomadic, Inc. (SensíQ®). For instance, SensíQ® Pioneer uses an SPR detector sensitive to < 1 x 10^{-7} refractive index units that can monitor fast binding/dissociation interactions of very small (<100 Da) or large analytes (>1 μm particle) over a very broad range of affinities (pM–mM) [23].

2.1.2 Quartz Crystal Microbalance

QCM is an ultra-sensitive weighing device that utilizes the mechanical resonance of piezoelectric single-crystalline quartz [24]. In the most common configuration, a thin circular crystal disc is sandwiched between a pair of circular metal electrodes (usually gold). By applying an AC voltage, resonance is excited when the frequency of the applied voltage corresponds to the natural resonance frequency, f_0, of the crystal. This resonance occurs when the thickness of the disc is an odd integer number of half-wavelengths of the standing wave induced between the electrodes, causing the mechanical oscillation to have its anti-nodes at each electrode interface. The resonance frequency change, Δf is thus proportional to the changes in mass of the crystal, Δm as expressed in the Sauerbrey equation

$$\Delta f = -\frac{2 f_0^2}{A\sqrt{\mu_q \rho_q}} \Delta m \tag{4}$$

where A (cm^2) is the area of the electrode surface, ρ_q (g/cm^3) and μ_q ($g/cm \cdot s^2$) are the density and shear modulus of the quartz, respectively.

The use of QCM technique to probe DNA immobilization and DNA hybridization was pioneered by Okahata and co-workers, where specific-sequence hybridization is detected within a circular M13 phage DNA molecule [25] and was later extend to studies of template-directed DNA synthesis [26]. At the same time, Storri et al. demonstrated 23-mer DNA oligonucleotide hybridization at sensitivity of 0.5 μM using QCM [27]. The merit of the QCM technique comes from the fact that properly oriented DNA on a planar interface adopts a structure which can bind to a substantial amount of water. In fact, up to 90% of the measured mass originates from coupled water, which in turn makes the technique more sensitive than optical techniques. However, like SPR, QCM has the drawback of being very temperature sensitive. The detection limit is still in the order of 10^{-8} g/cm^2 even at the usage of a temperature controller [26], makes it difficult for detection of DNA single-base extension reaction where the mass change is approximately 2.0×10^{-9} g/cm^2 for a DNA density of 4×10^{12} molecules/cm^2.

2.2 Label-free (2): Electrochemical

When dissolve in a solution, each phosphate group that comprises the backbone of the DNA is ionized to carry one negative electronic charge. The formation of a double-stranded DNA from a

single-stranded probe DNA due to hybridization increases, in particular doubles the charges to give variation in electrochemical properties (i.e. current/potential, impedance, etc.) [28]. Electrochemical DNA biosensors can employ potentiometric, amperometric or impedimetric transducers to convert the electrochemical reactions into a measurable electrical signal directly. Hence, biosensors based on this approach greatly simplify signal transduction, avoiding expensive equipment requirement. Furthermore, the advanced progress of today microfabrication technology can offers enormous advantage, especially in miniaturization for a portable and affordable POC device.

2.2.1 Potentiometric

Many potentiometric biosensors are based on the principle of ion sensitive field effect transistor (ISFET) developed by Bergveld in 1970 [29]. As illustrated in Fig. 2.2, the structure of ISFET is slightly different with conventional metal-oxide semiconductor field-effect transistor (MOSFET), where the metal gate of the MOSFET is replaced by the metal of a reference electrode in contact with the electrolyte. In ISFET, ion-selective membrane is attached to the gate insulator material of the transistor and the presence of charge at the interface will induce a change in charge density of opposite sign in the space-charge region of the semiconductor, thus causes a change in the current that flows in the channel. The effect is essentially the flat-band voltage shift, V_{FB} [30] that can be expressed by

$$V_{FB} = E_{ref} - \psi_0 + \chi_{sol} - \frac{\Phi_{Si}}{q} - \frac{Q_{ss} + Q_{ox}}{C_{ox}} \tag{5}$$

with E_{ref} the reference electrode potential relative to vacuum, ψ_0 the surface potential, χ_{sol} the surface dipole potential of the solution, Φ_{Si} the silicon work function, q the electron charge, Q_{ss} the surface state density at the silicon surface, Q_{ox} the fixed oxide charge, and C_{ox} the gate insulator capacitance per unit area. Since all terms are constant except ψ_0, the change of the surface potential generated by surface ions then can be detected by measuring the changes in flat-band voltage.

In the case of DNA biosensor, the ion-selective membrane is substituted by a probe DNA monolayer as the recognition element. The increase of negative charges upon the hybridization process of DNA caused the cations to accumulate, which leads to charge redistribution on the surface and modulates the gate voltage accordingly. The first attempt to detect label-free DNA hybridization

using silicon ISFET was carried out by Souteyrand et al. [31]. Since then, numerous works using various materials to build the transistors have emerged. Uslu et al. attached 20-mer probes onto a Si/SiO_2 structure silanised with 3-Aminopropyltriethoxysilane (3-APTES) and detected hybridization by monitoring changes in the gate voltage [32]. Kamahori et al. employed $Si/SiO_2/Si_3N_4/Au$ structure in their design with the probe was chemisorbed on a gold layer and sensed the occurrence of hybridization by measuring a shift in the drain-source characteristic (I_{DS}-V_{DS}) curve [33]. The disadvantage of ISFET biosensor in measuring the biomolecular recognition is the issue of the Debye screening length. Since the biosensing only can take place within the Debye length, which is approximately 10 nm from the gate surface, detection for DNA hybridization at the distance beyond the Debye length is not possible.

2.2.2 Amperometric

Most of ready-to-use electrochemical biosensors today are based on the monitoring of electron-transfer processes, so-called amperometric sensors [34]. Typically, label-free amperometric biosensors involve the use of solution-borne reporter molecules (i.e. electroactive species) and chronoamperometry technique to monitor the faradaic current generated by electrochemical reactions at the electrode as the potential is kept constant. In amperometric DNA biosensors as shown in Fig. 2.3, a single-stranded probe is tethered to a working electrode to capture its complementary strand (target DNA). When target is captured, the accumulation of electroactive species near the sensing electrode results in a measurable redox current. As the current change registered is proportional to the amount of DNA on the electrode, monitoring before and after hybridization can report on occurrence of hybridization. Amongst amperometry-based label-free works, Millan and Mikkelsen have reported DNA hybridization using sequence-selective biosensor with $Co(phen)_3^{3+}$ as electroactive species [35]. Although label-free amperometric sensors suffer from low detection limit, it can be improved by utilizing peptide nucleic acid (PNA) as a capture probe instead of DNA due to the fact that PNA is neutral in charge hence minimize the accumulation of electroactive species on probe-tethered electrode [36]. The main drawbacks of amperometric biosensors are high applied potential and interference with nonspecific electroactive particles.

2.2.3 Impedimetric

Other types of electrochemical biosensors that rely on surface property changes are impedimetric sensors. It is important to note that, impedance sensors discussed here are restricted to cases in which the impedance (i.e. resistance, capacitance) of the biological layer itself is measured, even though impedance sensors operates by field-effect modulation, or in other words by means of channel conductance or capacitance of the electrolyte-insulator-semiconductor interface have been also proposed [37-40]. Impedance biosensors measure the electrical impedance of the electrode-solution interface by imposing a small sinusoidal voltage at a particular frequency and measuring the resulting current, where the ratio of current to voltage gives the impedance. There are two types of impedance sensors. One is faradaic biosensor in which involve the use of redox active species to induce passage of current (i.e. charge transfer) across the interface. The second is nonfaradaic biosensor that is totally opposite in process, by not involve any use of redox but only the flow of transient current (e.g. charging/discharging the interfacial capacitor), thus usually refers to the capacitance biosensor.

Faradaic impedance biosensors often use the changes in the charge transfer resistance, R_{ct} at the working electrode surface to detect DNA hybridization. As depicted in Fig. 2.4, the electrical model of the interface can be represented by a double layer capacitance, C_{dl}, charge transfer resistance, R_{ct}, Warburg impedance, Z_W, and solution resistance, R_S. The transformation from single-stranded to double-stranded DNA upon hybridization increases the negative charge on the surface hindering the negatively-charged redox species to get nearer to the electrode as they are repelled by the electrostatic barrier of DNA, which results in a diminished rate of charge transfer (i.e. an increase in R_{ct}) [41-44]. For example, Alfonta and co-workers used the rejection of the ferricyanide/ferrocyanide ($Fe(CN)_6^{3-}/Fe(CN)_6^{4-}$) redox couple to demonstrate oligonucleotide DNA hybridization [45]. They showed from a Nyquist plot that the radius of semicircular is enlarged after hybridization indicating an increase in charge transfer resistance of the interface. Detection of a single-nucleotide mismatch was reported by Kraatz et al. [46] in which differences in charge transfer resistance between two different DNA duplex form (B-DNA and M-DNA) indicates the eight single-nucleotide mismatches within a 20-mer DNA sequence.

In contrast to faradaic biosensors, nonfaradaic biosensors strive to do away with redox molecules

in solution and rely solely to the electrical properties changes (i.e. C_{dl}) of the interface. Monolayer of DNA itself is an insulating dielectric ($\varepsilon_r \approx 2\text{-}5$) thus adsorption of DNA onto an electrode surface will cause a decrease in capacitance due to the increase in distance between the charges in the polarized electrode and the ions in the solution (i.e. layer thickness). A typical concept in nonfaradaic sensors is the formation of double-stranded DNA due to hybridization should increase layer thickness and/or decrease dielectric properties (i.e. ε_r) of the probe layer, both decreasing capacitance. Capacitance is usually determined by measuring the charging current generated by a voltage step excitation over one period, where the current integration, which essentially the charge on the capacitor divides with the magnitude of the voltage gives the capacitance. The feasibility of using capacitance measurement to detect DNA hybridization was pioneered by Berggren et al. [47]. The binding of 26-mer target to 8-mer oligonucleotide probes immobilized on a gold electrode was demonstrated using the potentiostatic step technique. A decrease in capacitance was observed and claimed to be due to the displacement of water and solvated ions from the electrode surface upon hybriridization. Guiducci et al. demonstrated hybridization using oligonucleotide probes that were attached on microfabricated gold electrode chips [48]. They observed the capacitance change interpreted by impedance data obtained from electrochemical impedance spectroscopy and showed that the capacitance has a frequency dependent (i.e. constant phase element) behavior. They also conducted a capacitance measurement using an external circuit setup based on charge-based capacitance measurement technique and observed a capacitance decrease of 28.5% after hybridization. Their impressive result has showing promise for fully on-chip integration of DNA capacitance biosensor that is desirable for POC applications.

2.3 Summary of comparisons

The pros and cons of current available label-free detection techniques are summarized in Table 1.

Table 1. Comparison of label-free DNA detection techniques.

Label-free detection techniques	Advantages	Limitations	Maturity or current status

SPR	Real time monitoring.	Difficult to improve signal-to-noise ratio since refractive index of measurement buffer is comparable to that of the target. Temperature sensitive.	Commercial product available (e.g.BIAcore, SensíQ®).
QCM	Real time monitoring.	Not compatible since probes need to be tehthered to piezo crystal. Temperature sensitive.	Commercial product available (e.g. Masscal, Maxtek RQCM, Akubio).
Field-effect	Simple readout. Scalable in size.	Real time is not possible (unless PNA probes are used). Detection fails at distance beyond Debye length.	Research is ongoing. High potential for POC device.
Amperometric	High sensitivity.	Need application of high potential. Require redox species.	Matured technology. Several commercial products to detect glucose are available.
Faradaic impedance	Simple structure. Simple readout. High sensitivity.	Require redox species.	Research is ongoing.
Nonfaradaic impedance (capacitance)	Simple structure. Simple readout. No redox involved.	Selectivity challenge in real-world (actual) biological sample as there are significant	Research is ongoing. Most amenable to POC-based diagnostics.

		amount of non-specific analyte in the samples.	

From above, it can be concluded that nonfaradaic impedance biosensing is the most attractive for POC device development due to its simple structure and direct signal transduction. Besides the possibility to integrate the sensor and readouts into a single chip, the absence of redox indicator gives an advantage of more precise and accurate measurement of detecting biomolecular interactions.

[**References**]

20. J. Homola, S. Yee, G. Gauglitz, *Surface plasmon resonance sensors: Review.* Sens. Act. B, 1999, 54, pp. 3-15.
21. www.discoversensiq.com, *Overview of surface plasmon resonance.* Nomadics, Inc., Oklahoma.
22. B. P. Nelson, T. E. Grimsrud, M. R. Liles, R. M. Goodman, R. M. Corn, *Surface plasmon resonance imaging measurements of DNA and RNA hybridization adsorption onto DNA microarrays.* Anal. Chem., 2001, 73 (1), pp. 1-7.
23. L. Flood, J. Havard, N. Gillock, A. Martin, J. Quinn, *Automated surface plasmon resonance-based biosensing.* Drug Discovery & Development, Jan., 2010.
24. F. Hook, M. Rudh, *Quartz crystal microbalances (QCM) in biomacromolecular recognition.* Review in Bti Molecular Biology. Feb-Mar., 2005, pp. 8-13.
25. Y. Okahata, Y. Matsunobu, K. Ijiro, M. Mukae, A. Murakami, K. Makino, *Hybridization of nucleic acids immobilized on a quartz crystal microbalance.* J. American Chem. Soc., 1992, 114, pp. 8299-8300.
26. K. Niikura et al., *Direct monitoring of DNA polymerase reactions on a quartz crystal microbalance.* J. American Chem. Soc., 1998, 120 (33), pp. 8537-8538.
27. S. Storri, T. Santoni, M. Mascini, *A piezoelectric biosensor for DNA hybridisation detection.* Anal. Lett., 1998, 31 (11), pp. 1795-1808.
28. M. Pohanka, P. Skladai, *Electrochemical biosensors – principles and applications.* J. Appl.

Biomed., 2008, 6, pp. 57-64.

29. P. Bergveld, *Development of an ion-sensitive solid-state device for neurophysiological measurements.* IEEE Trans. Biomed. Eng., 1970, 17, pp. 70-71.
30. P. Bergveld, *ISFET, Theory and Practice.* IEEE Sens. Conf., 2003, pp. 1- 26.
31. E. Souteyrand, J. P. Cloarec, J. R. Martin, C. Wilson, I. Lawrence, S. Mikkelsen, M. F. Lawrence, *Direct detection of the hybridization of synthetic homo-oligomer DNA sequences by field-effect.* J. Phys. Chem. B, 1997, 101, pp. 2980-2985.
32. F. Uslu, S. Ingebrandt, D. Mayer, S. Bocker-Meffert, M. Odenthal, A. Offenhausser, *Labelfree fully electronic nucleic acid detection system based on a field-effect transistor device.* Biosens. Bioelectron., 2004, 19, pp. 1723-1731.
33. M. Kamahori, Y. Ishige, M. Shimoda, *DNA detection by an extended-gate FET sensor with a high frequency voltage superimposed onto a reference electrode.* Analytical Sciences, 2007, 23, 1, pp. 75-79.
34. M. S. Belluzo, M. E. Ribone, C. M. Lagier, *Assembling amperometric biosensors for clinical diagnostics.* Sensors, 2008, 8, pp. 1366-1399.
35. K. M. Millan and S. R. Mikkelsen, *Sequence-selective biosensor for DNA based on electroactive hybridization indicators.* Anal. Chem., 1993, 65, pp. 2317-2323.
36. Z. Fang and S. O. Kelley, *Direct electrocatalytic mRNA detection using PNA-nanowire sensors.* Anal. Chem., 2009, 81, pp. 612-617.
37. F. Wei, B. Sun, Y. Guo, X. S. Zhao, *Monitoring DNA hybridization on alkyl modified silicon surface through capacitance measurements.* Biosens. Bioelectron., 2003, 18, pp. 1157-1163.
38. W. Cai, J. R. Peck, D. W. van der Weide, R. J. Hamers, *Direct electrical detection of hybridization at DNA-modified silicon surfaces.* Biosens. Bioelectron., 2004, 19, pp. 1013.
39. H. Berney, J. Alderman, W. Lane, J. K. Collins, *A differential capacitive biosensor using polyethylene glycol to overlay the biolayer.* Sens. Actuators B, 1997, 44, pp. 578-584.
40. V. Billard, C. Martelet, P. Binder, J. Therasse, *Toxin detection using capacitance measurements on immunospecies grafted onto a semiconductor substrate.* J. Anal. Chim. Acta, 1991, 249, pp. 367-372.
41. A. Bardea, F. Patolsky, A. Dagan, I. Wilner, *Sensing and amplification of oligonucleotide-DNA interactions by means of impedance spectroscopy: a route to a Tay-Sachs sensor.* Chem.

Commun., 1999, 1, pp. 21-22.

42. J. Kafka, O. Panke, B. Abendroth, F. Lisdat, *A label-free DNA sensor based on impedance spectroscopy.* Electochimica Acta, 2008, 53, 25, pp. 7467-7476.
43. S. D. Keighley, P. Estrela, P. Li, P. Mighorato, *Optimization of label-free DNA detection with electrochemical impedance spectroscopy using PNA probes.* Biosens. Bioelectron., 2008, 24, 4, pp. 906-911.
44. J. Y. Liu, S. J. Tian, P. E. Nielsen, W. Knoll, *In situ hybridization of PNA/DNA studied label-free by electrochemical impedance spectroscopy.* Chem. Commun., 2005, 23, pp. 2969.
45. L. Alfonta, I. Willner, *Electronic transduction of biocatalytic transformations on nucleic acid-functionalized surfaces.* Chem. Commun., 2001, 16, pp. 1492-1493.
46. X. Li, J. S. Lee, H. B. Kraatz, *Electrochemical detection of single-nucleotide mismatches using an electrode array.* Anal. Chem., 2006, 78, 17, pp. 6096-6101.
47. C. Berggren, P. Stalhandske, J. Brundell, G. Johansson, *A feasibility study of a capacitive biosensor for direct detection of DNA hybridization.* Electroanalysis, 1999, 11, 3, pp. 156-160.
48. C. Guiducci, C. Stagni, A. Fischetti, U. Mastromatteo, B. Ricco, *Microelectrodes on a silicon chip for label-free capacitive DNA sensing.* IEEE Sens. J., 2006, 6, 5, pp. 1084-1093.

2.4 Figures

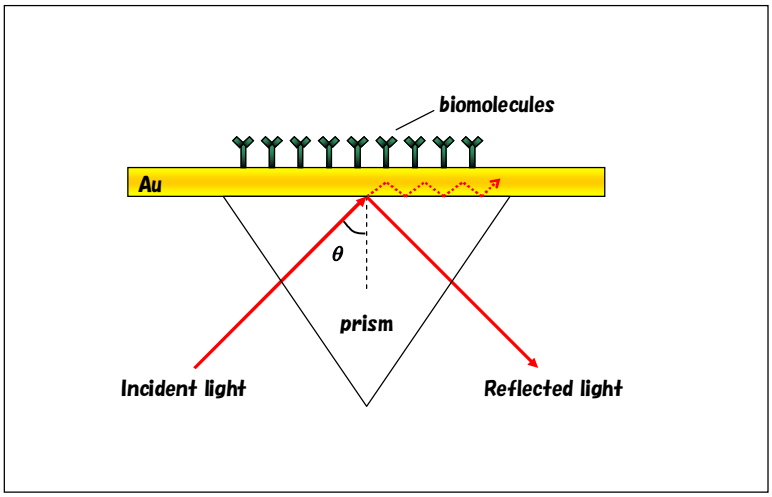

Fig. 2.1 Principle of surface plasmon resonance.

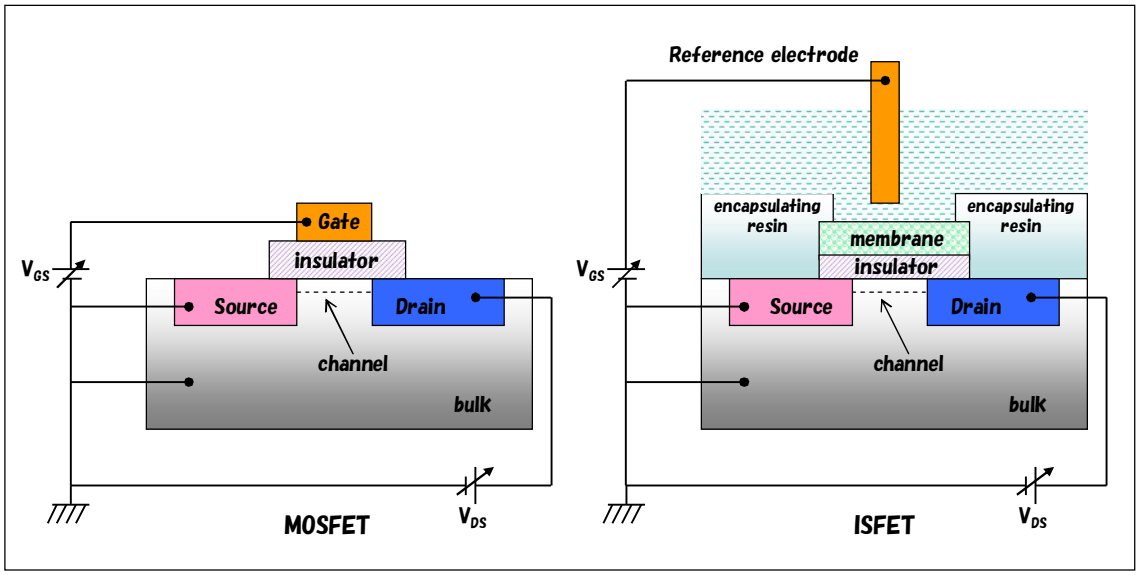

Fig. 2.2 Structure difference between MOSFET and ISFET.

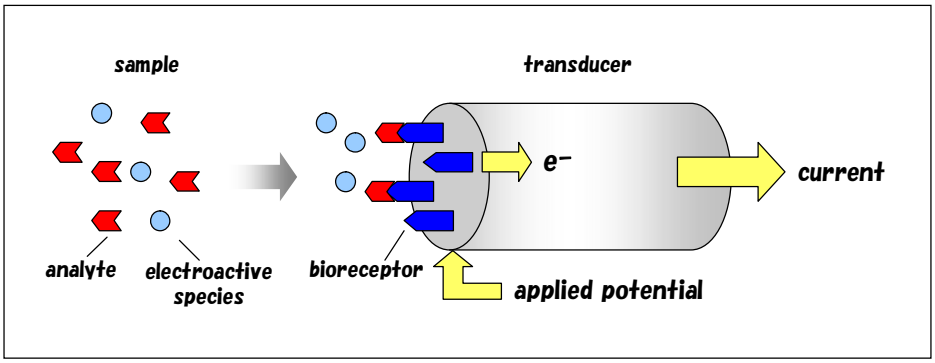

Fig. 2.3 Illustration of an amperometric biosensor.

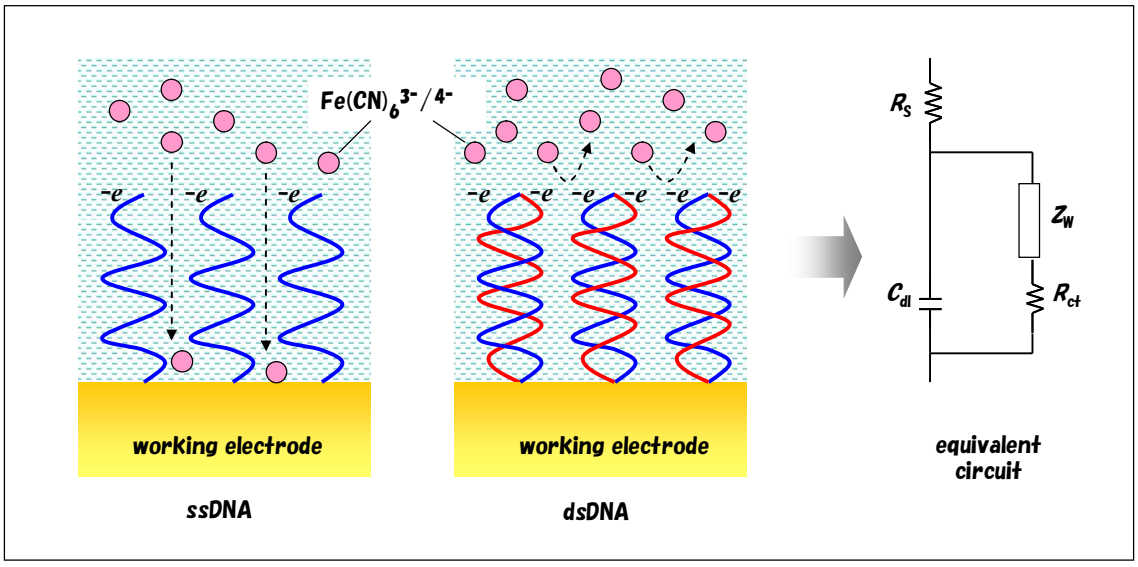

Fig. 2.4 Impedance measurement using negatively charged redox molecules.

Chapter 3

On-chip DNA detection

In this chapter, a biosensor chip based on nonfaradaic impedance measurement that exploited the changes in electrical double layer properties of the biomodified electrode is proposed. The feasibility of using an on-chip gold microelectrode with CMOS readout is demonstrated and the detection of DNA hybridization is carried out.

3.1 Electrode-solution interface

Since the sensing principle is relied on the changes of electrical double layer as a result of biomodification or biorecognition event, it is important to understand the interfacial electric phenomena that occur at metal electrode surface. The basic of electrical double layer, its equivalent circuit and how the biomodification at electrode surface will alter the double layer properties are briefly explained.

3.1.1 Electrical double layer

The double layer model is used to visualize the ionic environment in the vicinity of a charged surface. It can be either a metal under potential or due to ionic groups on the surface of a dielectric. The term 'electrical double layer' was originated from the model proposed by Helmholtz. In his model, he assumed that no electron transfer reactions occur at the metal electrode and the solution is composed only of electrolyte. The interactions between the ions in solution and the electrode surface were assumed to be electrostatic in nature and resulted from the fact that the electrode holds a charge density which arises from either an excess or deficiency of electrons at the electrode surface. In order for the interface to remain electrically neutral the charge held on the electrode is balanced by the redistribution of ions close to the electrode surface. The attracted ions (usually called counterions) are assumed to approach the electrode surface and form a layer balancing the electrode

charge, the distance of approach is assumed to be limited to the radius of the ion and a single sphere of salvation round each ion. The result is two layers of charge (layer of charge in metal electrode and layer of counterions in solution), called the electrical double layer and a potential drop that is linear with the separated distance, d (Fig. 3.1 (a)). This is the same as that of a simple parallel plate capacitor and thus the Helmholtz capacitance, C_{H} can be given by

$$C_{\mathrm{H}} = \frac{\varepsilon_0 \varepsilon_r}{d} \tag{6}$$

where ε_0 is the dielectric constant and ε_r the relative permittivity of water. However, the model of Helmholtz only accounts for the spatial charge distributions at a metal-solution interface with an assumption that ion diffusion rate is infinite, which is far from reality.

Later, Gouy and Chapman came with the theory that describes the physics of the diffuse part of the double layer. They proposed that counterions are not rigidly held, but behave as point charges in a diffuse cloud and the electrical potential decreases exponentially away from the electrode surface to the solution (Fig. 3.1 (b)). The relationship between the ion concentration, n_i and the potential, ϕ at x distance from the electrode is given by Boltzmann distribution law:

$$n_i(x) = n_i(\infty)\exp\left(-\frac{ez_i\phi(x)}{k_{\mathrm{B}}T}\right) \tag{7}$$

where e is the absolute value of electron charge, z_i the valence of ion, k_{B} the Boltzman constant, and T is the absolute temperature. Combining above equation with Poisson electrostatic law:

$$\frac{d^2\phi}{dx^2} = -\frac{\rho(x)}{\varepsilon_0\varepsilon_r} = -\frac{\sum z_i e n_i}{\varepsilon_0\varepsilon_r} = -\frac{e}{\varepsilon_0\varepsilon_r}\sum_i z_i n_i(\infty)\exp\left(-\frac{ez_i\phi(x)}{k_{\mathrm{B}}T}\right), \tag{8}$$

and solving for surface charge, σ yields

$$\sigma = \sqrt{2\varepsilon_0\varepsilon_r k_{\mathrm{B}}TN_A\sum_i M_i\left[\exp\left(-\frac{ez_i}{k_{\mathrm{B}}T}\phi_0\right)-1\right]}. \tag{9}$$

At $z_1 = z$, $z_2 = -z$, and $M_1 = M_2 = M$,

$$\sigma = \sqrt{8\varepsilon_0\varepsilon_r k_{\mathrm{B}}TN_A M}\,\sinh\left(\frac{ez}{2k_{\mathrm{B}}T}\phi_0\right), \tag{10}$$

where N_{A} is the Avogadro constant, M the molar concentration of ions in the solution and ϕ_0 the electrostatic surface potential. This equation is known as the Grahame equation.

Hence, the small signal capacitance of the diffuse double layer or so called Gouy-Chapman

capacitance, C_{GC} can be expressed as

$$C_{GC} = \frac{d\sigma}{d\phi_0} = \frac{\varepsilon_0 \varepsilon_r}{\lambda_D} \cosh\left(\frac{e\phi_0}{2k_B T}\right). \tag{11}$$

Here, λ_D denotes the Debye length that is defined as

$$\lambda_D = \sqrt{\frac{\varepsilon_0 \varepsilon_r k_B T}{2z^2 e^2 N_A M}}. \tag{12}$$

Gouy-Chapman approach is mathematically and physically equivalent to the more well-known Debye-Huckel theory of ion-ion interactions in solution and does not satisfactorily explain the observed variation of the capacitance with potential. The prediction is only valid in the vicinity of the potential of zero charge and fails at high electrolyte concentrations. Their model over-emphasizes the diffuse nature of the double layer and the assumption that there is no physical limit for the ions in their approach to the surface (i.e. ions are charges without size), is not realistic. In order to resolve this problem, Stern suggested the combination of the Helmholtz and Gouy-Chapman models, known as Gouy-Chapman-Stern model (Fig. 3.1 (c)). His theory states that ions do have finite size which includes their solvated shell. The inner layer comprises the absorbed solvent molecules and may sometimes specifically absorbed ions with the distance of approach is the radius of the absorbed ion (termed the inner Helmholtz plane, IHP). Counterions can approach the electrode only as far as their salvation sheath allows and the distance of closest approach is at the center of solvated ions (termed the outer Helmholtz plane, OHP). The region between IHP and OHP is called the Stern layer or compact layer in which the potential is assumed to vary linearly with the distance. A diffuse layer further from the wall applied the Gouy-Chapman theory, where the potential changes exponentially with the distance. In a simplified view of the Stern model, the double layer capacitance, C_{dl} can be regarded as being composed of two capacitances connected in series

$$\frac{1}{C_{dl}} = \frac{1}{C_H} + \frac{1}{C_{GC}}. \tag{13}$$

with C_H the Helmholtz capacitance of the Stern layer and C_{GC} the Gouy-Chapman capacitance of the diffuse layer. This result suggests that at high concentrations the interface becomes more like the simple capacitor, whereas at lower concentrations the effects of the diffuse layer become dominant.

3.1.2 Equivalent circuit in electrochemical modeling

The process at electrode-solution interface may be described by an equivalent circuit model as shown in Fig. 3.2. A widely used simple model is the Randles equivalent circuit, that includes double layer capacitance C_{dl}, electron-transfer resistance R_{ct}, Warburg impedance Z_W, and ohmic resistance of the electrolyte solution R_S. An electrode process is called nonfaradaic, if it does not involve charge transfer to or from the electroactive redox species. But processes such as adsorption and desorption can occur and the structure of the electrode-solution interface can change with changing potential or solution composition. Although charge transfer does not occur in a nonfaradaic process, a transient current flow is possible due to rearrangement of solution composition. This nonfaradaic charging current is modeled by the C_{dl} in the equivalent circuit. A resistive element to describe the barrier induced by double layer is represented by R_p (instead of R_{ct}), which is termed a polarization resistance and typically assumed to be infinite. A series of R_{ct} and Z_W describes the faradaic impedance. A faradaic process is a type of electrode process in which charges or electrons are transferred across the electrode-solution interface through chemical oxidation or reduction reactions. R_{ct} is purely resistive and describes the charge transfer resistance in the faradaic process. Both faradaic and nonfaradaic processes normally occur when electrode reaction takes place, therefore they are modeled as parallel elements in the equivalent circuit. Warburg impedance represents the diffusion of the applied redox species once the electron transfer gets started and R_S represents the bulk properties of the solution. Both R_S and Z_W are not affected by chemical transformations occurring at the electrode interface.

3.1.3 Capacitance change upon surface modification of biomolecules

As the focus of this work is to sense the non-faradaic impedance or capacitance variation after target DNA binding, the following simplified explanation should be able to provide an intuition into what we expect to see in the experiment. As an example, consider a gold electrode is modified with a layer of organic molecules such as alkanethiol self-assembled monolayer (SAM) and immersed in a salt solution with a given concentration. Fig. 3.3 shows a simplified scenario before and after addition of an alkanethiol monolayer onto the electrode surface. Upon deposition of the thiol

molecules on gold electrode through thiol-gold (SH-Au) chemistry, the double layer is shifted because of the new dielectric layer. Hence, the total capacitance of the modified interface (C_{INT}) can be presented as a combination of thiol monolayer capacitance (C_{layer}) and electrical double layer capacitance (C_{dl}) in series

$$\frac{1}{C_{INT}} = \frac{1}{C_{layer}} + \frac{1}{C_{dl}}. \tag{14}$$

Here, it should be noticed that there is a large difference between the relative permittivity of water (ε_r ~78) and that of a thiol monolayer (ε_r ~2-5). The low dielectric constant of the monolayer means that almost potential drop is occurred within this layer, resulting in significantly reduced double layer potential. Therefore, the capacitance of the double layer can be neglected thus gives

$$C_{INT} \approx C_{layer}. \tag{15}$$

If the electrode surface is assumed to be covered or passivated by thiol molecules in a very dense manner and concentration of solution used is high enough for C_{dl} in eq. (13) to act as a simple capacitor (i.e. Helmholtz capacitance, eq. (6)), the capacitance change after modification, ΔC ($= C_{INT} - C_{BARE}$) in comparison with a bare gold surface can be described by

$$\frac{\Delta C}{C_{BARE}} = \frac{\varepsilon_r''}{\varepsilon_r'} \cdot \frac{d}{d''} - 1 \tag{16}$$

where ε_r' is the dielectric constant of water, ε_r'' the dielectric constant of the monolayer, d the double layer thickness, and d'' is the monolayer thickness. According to above equation, one would expect a decrease in capacitance if any modifier (with dielectric constant smaller than ε_r') is introduced into the double layer.

For the case of interest here (DNA hybridization), the immobilization of probe DNA (modified to have a thiol group on their 5' end terminus) should decrease the capacitance of the interface as the dielectric constant has been reported to be about 1.9 [49, 50]. Further modification of this layer upon target capture is believed to change the layer thickness and the dielectric constant. Mearns et al. [51] reported an increase of layer thickness from 1 to 4~7 nm upon hybridization of 20-mer oligonucleotides. As for dielectric constant, the value goes up to 2.5 [49, 50] after complementary binding. Based on this information, hybridization of DNA is expected to cause the corresponding capacitance to undergo a further change (reduction). From this point of view, this work approach is based on the assumption that such a variation is independent of electrode potential, but only on

physical changes upon DNA hybridization.

3.2 DNA surface chemistry

Self-assembly is an attractive choice for the immobilization of probe molecules at surfaces, as the method is simple and allows a robust and densely packed configuration. Self-assembly refers to the attachment of head group of molecule with the surface of a support through an affinity chemical binding. Thiol (-SH) residue is the most common used head group to form a self-assembled monolayer (SAM) on gold substrates due to the high affinity of the sulfur for a gold and the high strength of the interaction between the two (i.e. coordinate-like bond, which the strength is about 45 kcal/mol). In order to immobilize DNA probes on the gold working electrodes using this self-assembly method, DNA oligonucleotides are modified to have a thiol group on their 5' end terminus [52]. Upon deposition on gold electrodes, thiolated terminal of the molecules are chemisorbed on the substrate, while the DNA portion of the molecules are standing parallel to each other and away from the substrate forming a SAM. Tarlov and co-workers [53] have developed a procedure for DNA immobilization of thiolated capture probes solution on a gold surface. Their surface chemistry is simple without steric hindrance. They stated that the probes can be adsorbed on the surface specifically through the sulfur atom and nonspecifically through the nucleotide bases. They suggested that nonspecific adsorption can be effectively removed by a subsequent immobilization of a back-filler such as alkanethiols and higher buffer concentration could give better coverage of probes on the gold surface as the high ionic strength is believed to suppress the intermolecular electrostatic repulsion between neighboring strands of DNA molecules. Their method has become the basis for the state-of-the-art platform for sequence specific DNA biosensors.

3.3 Charge-based capacitance measurement

The capacitance of DNA biomodified electrode has been reported to be approximately 1-20 $\mu F/cm^2$ [54-56]. To perform on-chip monitoring of DNA hybridization using gold microelectrodes, a method capable to sense a capacitance in the range of 10^2 to 10^3 femto-Farad (10^{-15} F) is required. Among the available methods, charge-based capacitance measurement (CBCM) has been chosen in

this work since it has enabled on-chip measurement of femtofarad capacitances with atto-Farad (10^{-18} F) resolution [57]. The principle of this technique is to charge and discharge the capacitance under test using a known step voltage at an appropriate frequency and calculate the target capacitance from the measured average current. The basic structure is illustrated in Fig. 3.4. It consists of a simple CMOS pseudo-inverter driven by two non-overlapping clock pulses to ensure that either of the two transistors conducts current ('on' state) at any given time. When the PMOS transistor (switch 1, S_1) is turned on, current from the supply voltage, V_{DD} will charge up the capacitance to be measured, C_X to have a charge of

$$Q_X = C_X V_{DD} . \tag{17}$$

Then, Q_X will be subsequently discharged into the ground when PMOS transistor is turned off and NMOS transistor (switch 2, S_2) subsequently turned on. Therefore, at one period of the clock pulse, the charge difference is equivalent to eq. (17), denoting that the transient (charging or discharging) average current, I_{Ave} at switching frequency, f can be expressed as

$$I_{Ave} = f C_X V_{DD} . \tag{18}$$

Accordingly, C_X can be extracted since V_{DD} and f are known parameters.

This technique is advantageous because it is easy to implement and the signal can be further converted into digital signal to allow data processing and biosensor to be integrated on a single CMOS chip.

3.4 Chip

A proposed biosensor with on-chip gold microelectrodes and CMOS circuitry are presented. Chip fabrication is done using 1.2 μm, 2-metal, 2-poly, CMOS technology and gold electrode preparation is explained.

3.4.1 Sensing principle

As shown in Fig. 3.5, two-electrode system can be used to perform the detection of the capacitance variations of the electrode interface. This technique exploits a change in total capacitance between two electrodes that are arranged in a planar configuration. The elimination of a

reference electrode offers simplicity and particularly, fabrication cost down. Referring back to Fig. 3.5, the topmost metal layer forms the sensing electrodes. The top passivation layer is removed through the use of via in standard dry etching CMOS fabrication process. The exposed sensing electrodes are then deposited with a noble metal such as gold (Au) since it is inert and chemically stable in electrolyte solution. The surface of one of the gold electrodes is modified with DNA probes/targets and another one is left unmodified or bare to act as a dummy electrode. The interface between the two electrodes can be represented by series of two different capacitances C_{INT} and C_{dl}, and the solution resistance R_S. Polarization resistance R_p is exempted in the figure as it is assumed to be infinite in nonfaradaic operation. As previously described (in Section 3.1.3), the capacitance of the modified electrode will dominate the total capacitance (refer eq. (15)). By monitoring the variation of total capacitance before and after DNA probe/target modification, the occurrence of DNA immobilization/hybridization can be detected.

3.4.2 Circuit architecture

The schematic of the sensor circuit is shown in Fig. 3.6. In order to have a sufficient sensor dynamic range (up to 70 dB), a differential CBCM structure consists of two matched configuration driven by the same signals is adopted. One is loaded to target capacitance (C_{target}) and the other is kept unloaded to provide a reference to compensate the parasitic capacitances, include stray capacitance (C_{stray}) from the electronics and the standing capacitance ($C_{standing}$) of the sensing electrodes, which may caused a capacitive offset at the input. The total capacitance at node x_1 can be expressed as

$$C_{X1} = C_{target} + C_{stray} + C_{standing} . \quad (19)$$

The use of an identical sensing electrode at a reference side makes the capacitance at node x_2 as a total of C_{stray} and $C_{standing}$:

$$C_{X2} = C_{stray} + C_{standing} . \quad (20)$$

Therefore, the differential input capacitance, ΔC_X can be given by

$$\Delta C_X = C_{X1} - C_{X2} = C_{target} . \quad (21)$$

This compensation scheme has the advantage on dynamic range, but at the cost of a larger sensor size. The employment of a fully differential current-to-voltage converter (IVC) at readout stage

further improves sensor resolution by suppressing correlated electronic noise and thus contributes for better sensor sensitivity.

The sensor operation is based upon CBCM principle. Complimentary switches composed of parallel PMOS and NMOS transistors (S_1, S_2, S_3) are used instead of the series PMOS and NMOS of pseudo-inverter in Fig. 3.4 to overcome the charge injection effect resulting from the charge accumulation under the gate of transistor during switch on and off states, as well as to reduce the clock feedthrough effect. When a voltage step is applied to the electrodes, the average transient current, I_X at each CBCM front-end can be defined as

$$I_{X(1,2)} = f\, C_{X(1,2)} \left(V_P - V_{CM}\right). \tag{22}$$

where V_P and V_{CM} are two different reference voltages and f=1/T is the sensing cycle frequency.

The readout IVC circuitry consists of a switched-capacitor integrators and a differential operational amplifier. The integrating capacitors, C_i integrate the output currents over a period of S_2 are on (sense mode). During S_1 are on and S_2 are off (reset mode), the integrated voltages are amplified at operational amplifier and the differential output voltage, ΔV_{OUT} can be expressed as

$$\Delta V_{OUT} = V_o^+ - V_o^- = \frac{A}{C_i + AC_i} \int (I_{X1} - I_{X2})\, dt \tag{23}$$

where A is the gain of operational amplifier. At stable state, the relationship between differential output voltage and differential input capacitance is given by

$$\Delta V_{OUT} = \frac{A}{C_i + AC_i} \left(V_P - V_{CM}\right) \Delta C_X . \tag{24}$$

Fig. 3.7 illustrates a transistor-level schematic of the operational amplifier with a self-biasing circuit. It consists of a two-stage differential amplifier that share the same common-mode feedback circuit (M15-M19). The common-mode voltage is held at a reference voltage V_{CM} and the feedback is achieved by controlling the bias voltages of tail-current transistors, M3 and M10. The gain and phase characteristics of the optimized OA circuit in a standard 1.2 μm CMOS technology are shown in Fig. 3.8. The power supply voltages are V_{DD}=+2.5 V and V_{SS}=-2.5V. The overall sensor circuit performance was evaluated for a differential input capacitance range of 1 to 10^4 fF, with a voltage step of 0.25 V and a clocking frequency of 100 kHz. The input standing capacitance of 10 fF is included in the simulation, and the values of C_i and the output load capacitance, C_L are set to 14 and 500 fF, respectively. Fig. 3.9 shows the lin-log plot of the differential output voltage versus

differential input capacitance. It can be observed that the circuit operates reasonably linear in the target range (1-10^3 fF) and reaches saturation of higher values of input capacitance due to the nonlinearity of the differential amplifier. The sensor sensitivity in the linear region is approximately 3 mV/fF. The circuit has been fabricated using a 1.2 μm, 2-metal, 2-poly, CMOS technology by ON Semiconductor Technology Japan for operation with a 5 V supply. A microphotograph of the sensor is shown in Fig. 3.10 and the area is 130 x 200 μm^2.

3.4.3 Chip preparation

Planar microelectrodes with the dimension of 4 x 4 μm^2 have been fabricated using the topmost metal (Metal2) layer and only the passivation layer on top of the electrodes that will be exposed to solution or biomodified (i.e. loaded with target capacitance, C_{X1}) are removed through the use of via in standard chip fabrication process. Chemical cleaning of the chip in ultrasonic bathing is performed before the postprocess is begun. The gold deposition and pattering process of the electrode are carried out using in-house thermal vapor deposition chamber and conventional lithography process as illustrated in Fig. 3.11. A 20-nm-thick layer of titanium is first deposited, followed by a 300-nm-thick layer of gold. Titanium is used in order to improve the adhesion between the electrode (Metal2) and the gold. Gold patterning is then carried out using optical lithography and wet etching techniques. The microphotograph of the deposited gold electrode is shown in Fig. 3.12 (a). Wire bonding with ceramic packaging is done at the vendor and after received, the sensing site (i.e. gold electrode's area) is exposed by placing a special-cut silicone sheet on it with the surrounding area covered by silicone resin for electrical isolation (Fig. 3.12(b)).

3.5 Measurement

3.5.1 Measurement setup

The instrumentation for on-chip measurement is shown in Fig. 3.13. Power supply and voltage reference signals are provided by an HP 4142B (Agilent Technologies) modular dc source/monitor, which is also used for output data reading. An HP 8131A (Agilent Technologies) pulse generator is

used to generate the nonoverlap clock signals. PC controls all the parameters involved in the measured and records the measurement data using LabView software (National Instruments). All measurements are carried out at a power supply of V_{DD}=+2.5 V, and V_{SS}= -2.5 V. The reference voltages V_P, V_B, and V_{CM}, are set at 0.5, 0.25, and 0 V, respectively.

3.5.2 Chemicals and apparatus

All the chemicals used are purchased from Kanto Chemical. Aqueous sodium chloride (NaCl) solutions of five different concentrations from 0.1 mM to 1 M are prepared using deionized (DI) Milli-Q water. A pH 7.0 potassium phosphate buffer solution (PBS) composed of 1 mM tripotassium phosphate (K_3PO_4), 1 mM NaCl, and 1 μM ethylene-diamine-tetraacetic acid (EDTA) is prepared. Acetone, isopropanol (IPA), and ethanol are used for chip cleaning. To reduce the measurement drift due to the penetration of air vapor into the solution, nitrogen bubbling of each solution is performed prior to measurement, and a glass slide is also employed to prevent air penetration during the measurement. In addition, a liquid container is designed and set on top of the chip to increase the solution volume and minimize the effect of the air penetration as shown in Fig. 3.14.

For DNA measurement, the thiol-modified 20-mer single-stranded (probe) oligonucleotides (5'-HS-$(CH_2)_6$-GGGAAAAAAAAAAAAAAGGG-3') and its complimentary single-stranded (target) oligonucleotides (5'-CCCTTTTTTTTTTTTTTCCC-3') are purchased from Hokkaido System Science, Japan. Self-assembly method is used in probe immobilization [53]. A concentration of 1 μM thiolated probes are dissolved in PBS and then spread on the gold electrodes to form the probe layer. After 6 h of exposure at room temperature, the chip is rinsed twice with the PBS to remove the unattached probes. For hybridization, the dissolved 1 μM target oligonucleotides in PBS are manually spotted onto the immobilized gold electrodes using a micropipette and the temperature is increased to 70 °C during hybridization for about 30 min to increase the reassociation rate. The chip is then cooled to room temperature for 1 h, and finally washed thoroughly in PBS to remove the unbound targets.

3.5.3 Sensor characterization

The feasibility of the proposed sensor to sense the double layer changes is verified by measurement using various concentrations of NaCl solution. Fig. 3.15 shows the measured result of differential output voltage (ΔV_{OUT}) against solution concentration at a various frequencies setting. It can be observed that the voltage increases as the concentration increases, as expected. According to eq. (12), double layer thickness decreases with increasing concentration, which results in the increase in capacitance and transient current/output voltage as well. The sensor response also shows similarity with the simulation result (Fig. 3.9). The frequency dependence of the differential output voltage and capacitance are shown in Fig. 3.16 and Fig. 3.17, respectively. It can be observed that the output voltage/capacitance decreases as the frequency increases, showing deviations from ideal capacitive behavior. This can be attributed to the dielectric dispersion of an aqueous solution at high frequency [58]. These results imply that the double layer capacitor of the first approximation model (Fig. 3.5) is best represented by a frequency dependent capacitor, a so-called constant-phase element (CPE). To affirm this, a capacitance measurement at various concentrations of NaCl solution using commercially available liquid test fixture with larger electrodes (Agilent Technology 16452A (Figure 3.18)) is performed. The data is measured using a precision impedance analyzer (Agilent Technology 4294A) for the frequency range from 40 Hz to 110 MHz. The result is shown in Fig. 3.19, where a frequency dependent capacitive behavior can be observed. The capacitance decreases as the frequency increases and, at high frequencies, the capacitance saturates, showing a good agreement with the sensor characteristic discussed earlier.

3.5.4 DNA detection

When probe oligonucleotides are immobilized on the electrode surface, a self-assembled monolayer serving as an insulator is formed in conjunction with the double layer. The resulting interfacial capacitance then is a total of these series capacitances. When complimentary targets are introduced to the probes, hybridization occurred and the interface properties (i.e., double layer thickness, dielectric constant, etc.) are altered, causing the corresponding capacitance to undergo a further change. DNA detection is demonstrated by comparing the results of the capacitance measurements using bare, immobilized, and hybridized electrodes as shown in Fig. 3.20. As can be observed, the immobilization caused a significant capacitance reduction when 20-mer thiolated

oligonucleotides are tethered on the gold surface. This is consistent with eq. (14) and eq. (15), thereby causing the total capacitance to decrease substantially. A further 20% reduction (10 fF) in capacitance is also observed after hybridization implies that the double layer has changed due to the hybridization event. The capacitance decrease upon hybridization may be due to ion displacement that caused the electrical double layer thickness to increase thus decrease the total capacitance [55, 59] and/or a change in the dielectric constant [49, 50]. This result confirmed that the immobilization and hybridization of DNA can be detected using 4×4 μm^2 on-chip electrode by monitoring the capacitance variations of electrode-solution interface. However, further investigation of electrochemical model to describe the real behavior of a hybridized DNA surface is necessary to improve data interpretation in DNA capacitance detection.

3.6 Conclusions

A capacitive biosensor is proposed, with possibilities to detect specific oligonucleotides with gold electrodes fabricated to microscale size. Experimental results using several concentrations of NaCl clearly demonstrate that the sensor featuring a fully differential CBCM and readout circuitry is feasible for a fully electrical biorecognition system. The results also show that both the immobilization and hybridization of DNA can be detected by monitoring the electrical double layer capacitance change. It is considered to represent a significant step toward the implementation of a label-free, fully integrated biosensor particularly for DNA detection.

[**References**]

49. K. A. Peterlinz, R.M. Georgiadis, Observation of hybridization and dehybridization of thiol-tethered DNA using two color surface plasmon resonance spectroscopy. J. Am. Chem. Soc., 1997, 119, pp. 3401-3402.
50. Z. Yang, I. Enquist, M. Wirde, J. M. Kauffman, U. Gelius, B. Liedberg, Preparation and characterization of mix monolayer assemblies composed of thiol analogues of cholesterol and fatty acid. Langmuir, 1997, 13, pp. 3210-3218.
51. F. J. Mearns, E. L. S. Wong, K. Short, D. B. Hibbert, J. J. Gooding, DNA biosensor concepts

based on a change in the DNA persistence length upon hybridization. Electroanalysis, 2006, 18, pp. 1971-1981.

52. B. J. Taft, M. O'Keefe, J. T. Fourkas, S. O. Kelley, *Engineering DNA-electrode connectivities: manipulation of linker length and structure*. Anal. Chim. Acta, 2003, 496, pp. 81-91.
53. T. M. Herne, M. J. Tarlov, *Characterisation of DNA probes immobilized on gold surfaces.* J. Am. Chem. Soc., 1997, 119, 38, 8916-8920.
54. R. P. Janek, W. R. Fawcett, A. Ulman, Impednace spectroscopy of self-assembled monolayers on Au(111): Evidence for complex double layer structure in aqueous NaClO4 at the potential of zero charge. J. Phys. Chem. B, 1997, 101, 42, pp. 8550-8558.
55. C. Berggren, P. Stalhandske, J. Brundell, G. Johansson, *A feasibility study of a capacitive biosensor for direct detection of DNA hybridization.* Electroanalysis, 1999, 11, 3, pp. 156-160.
56. M. Riepl, V. M. Mirsky, I. Novotny, V. Tvarozek, V. rehacek, O. S. Wolfbeis, *Optimization of capacitive affinity sensors: Drift suppression and signal amplification.* Anal. Chem. Acta, 1999, 392, 1, pp. 77-84.
57. J. C. Chen, D. Sylvester, C. Hu, *An on-chip, interconnect capacitance characterization method with sub-femto-farad resolution.* IEEE Trans. Semicond. Manuf., 1998, 11, 2, pp. 204-210.
58. J. Hong, D. S. Yoon, M. I. Park, J. Choi, T. S. Kim, G. Im, S. Kim, Y. E. Park, and K. No, *A dielectric biosensor using the capacitance change with AC frequency integrated on glass substrates.* Jpn. J. Appl. Phys., 2004, 43, pp. 5639-5645.
59. C. Guiducci, C. Stagni, G. Zuccheri, A. Bogliolo, L. Benini, B. Samori, B. Ricco, *DNA detection by integrable electronics.* Biosens. Bioelectron., 2004, 19, pp. 781-787.

3.7 Figures

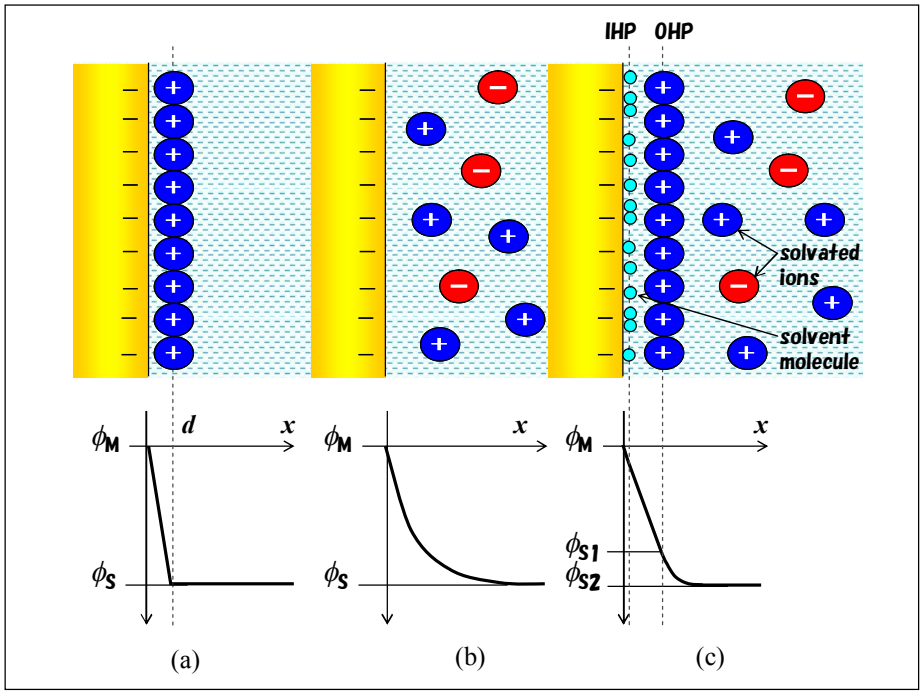

Fig. 3.1 Illustration of electrical double layer based on (a) Helmholtz theory, (b) Gouy-Chapman theory, and (c) Gouy-Chapman-Stern theory.

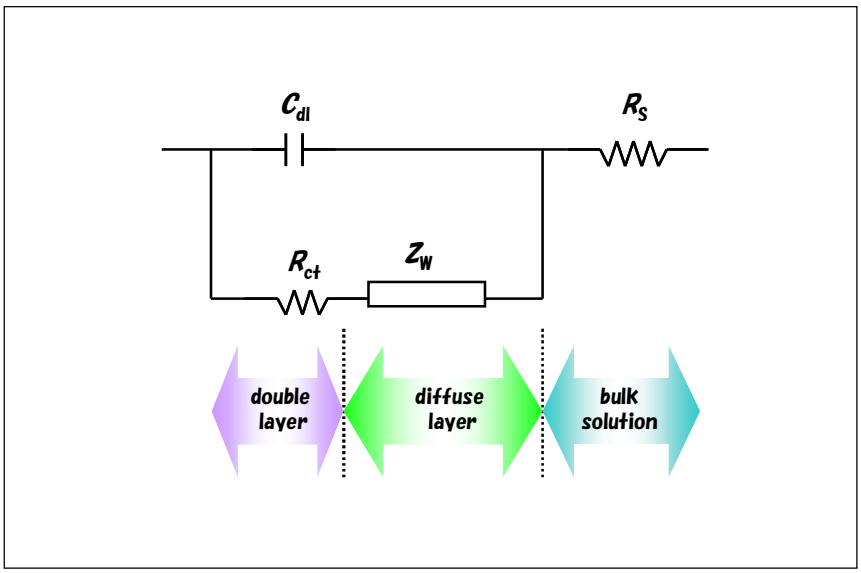

Fig. 3.2 Randles equivalent circuit to model electrode-solution interface.

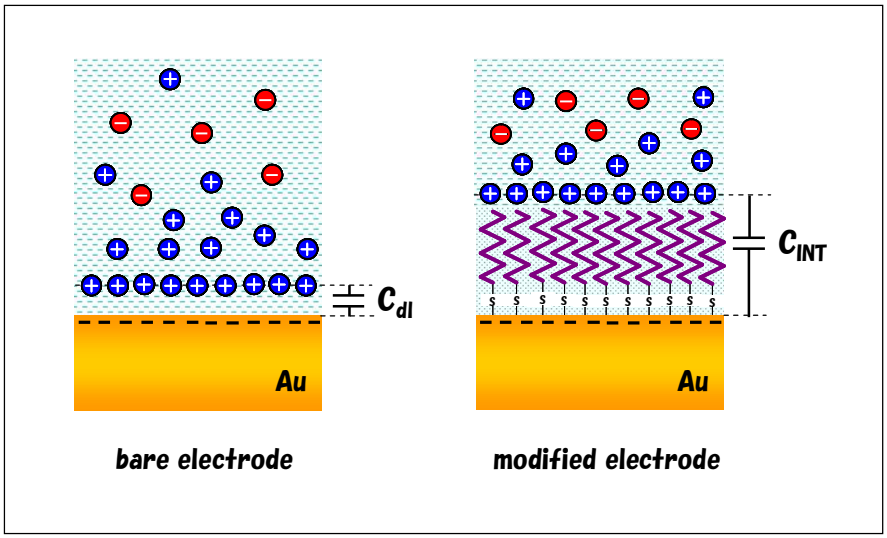

Fig. 3.3 Simple representation of a gold surface upon modification with an alkanethiol monolayer.

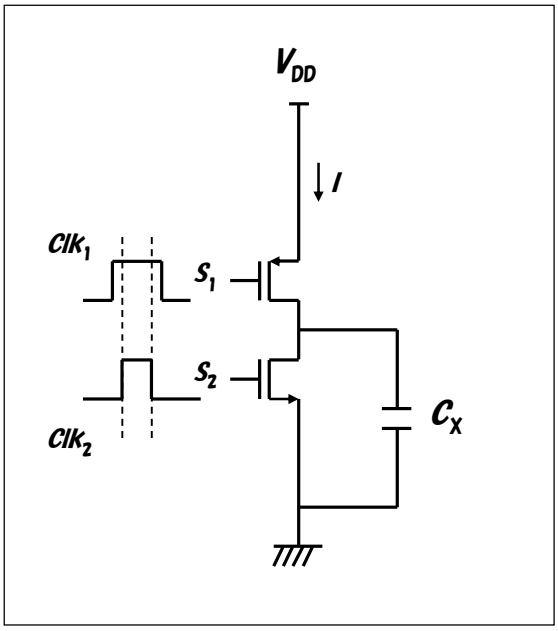

Fig. 3.4 Basic circuit of charge-based capacitance measurement .

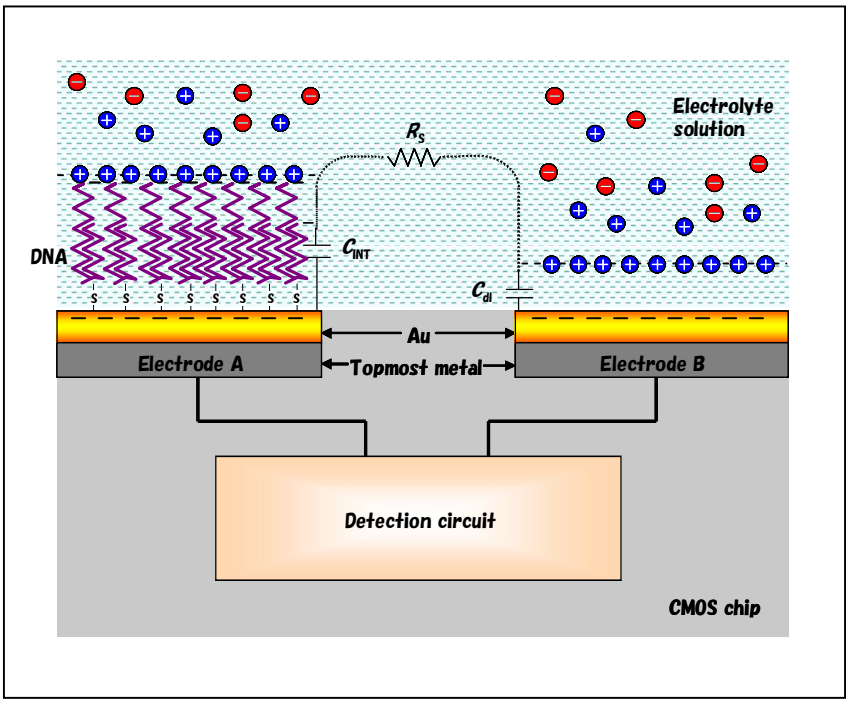

Fig. 3.5 Principle of on-chip DNA sensing.

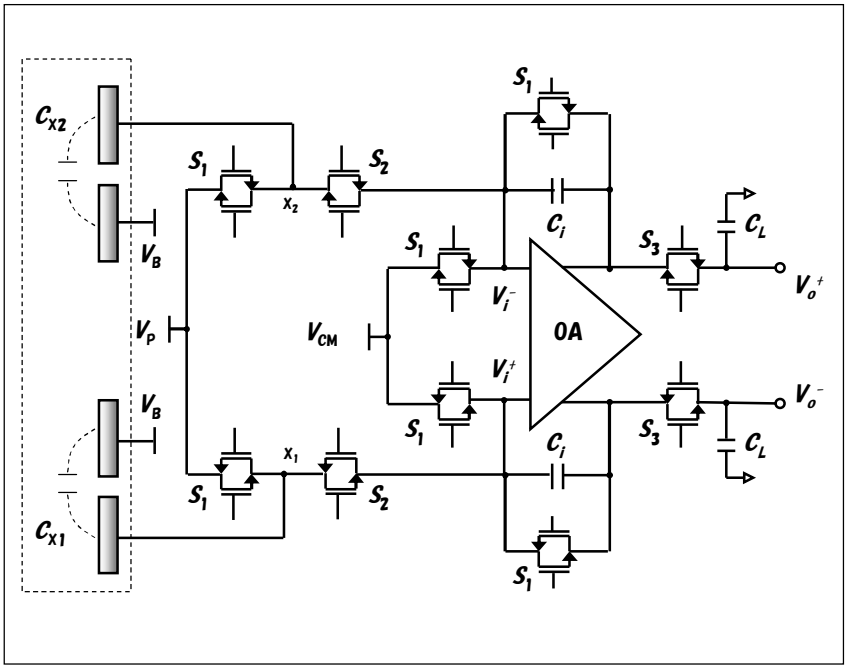

Fig. 3.6 Schematic of a fully differential sensor circuit.

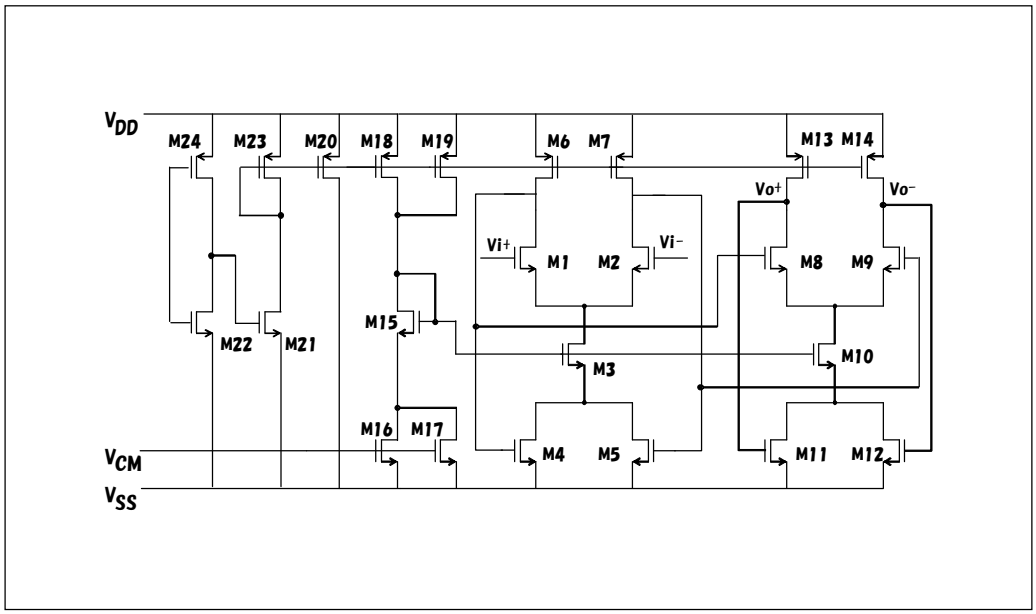

Fig. 3.7 Transistor-level schematic of self-biasing operational amplifier.

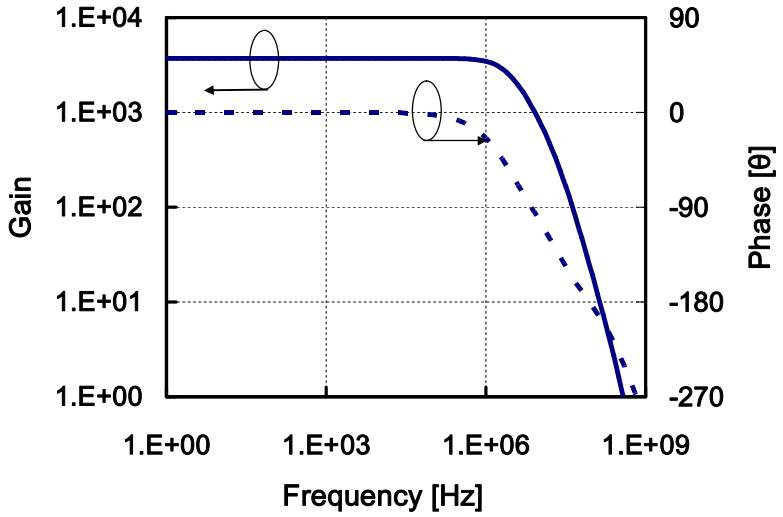

Fig. 3.8 Gain and phase characteristics of operational amplifier.

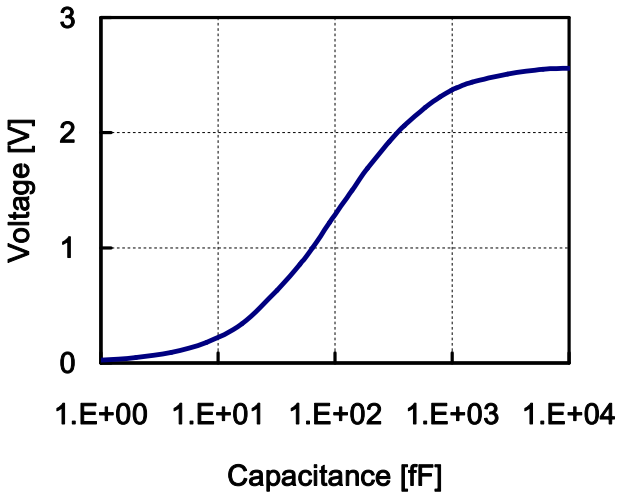

Fig. 3.9 Transfer characteristic of proposed sensor.

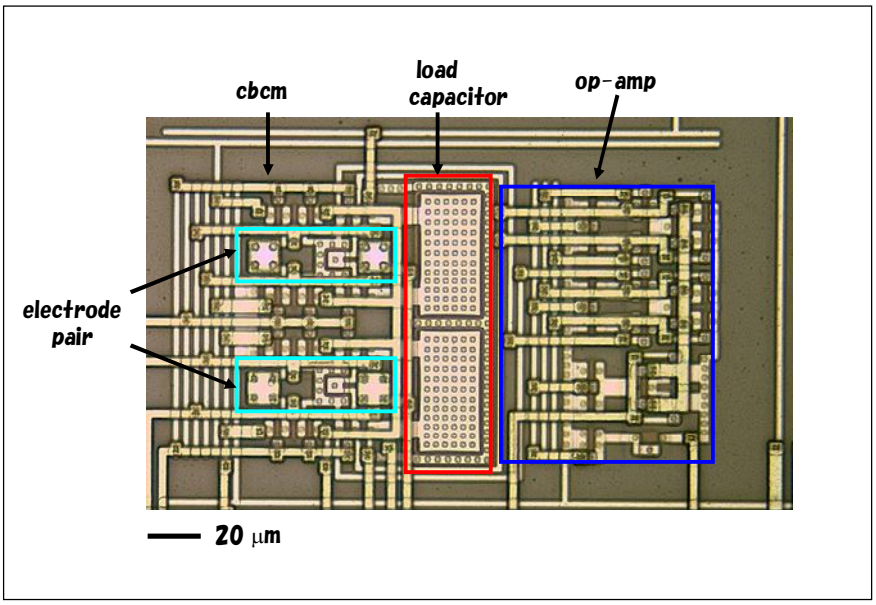

Fig. 3.10 Photomicrograph of a fabricated sensor. The area is 200 × 130 μm^2.

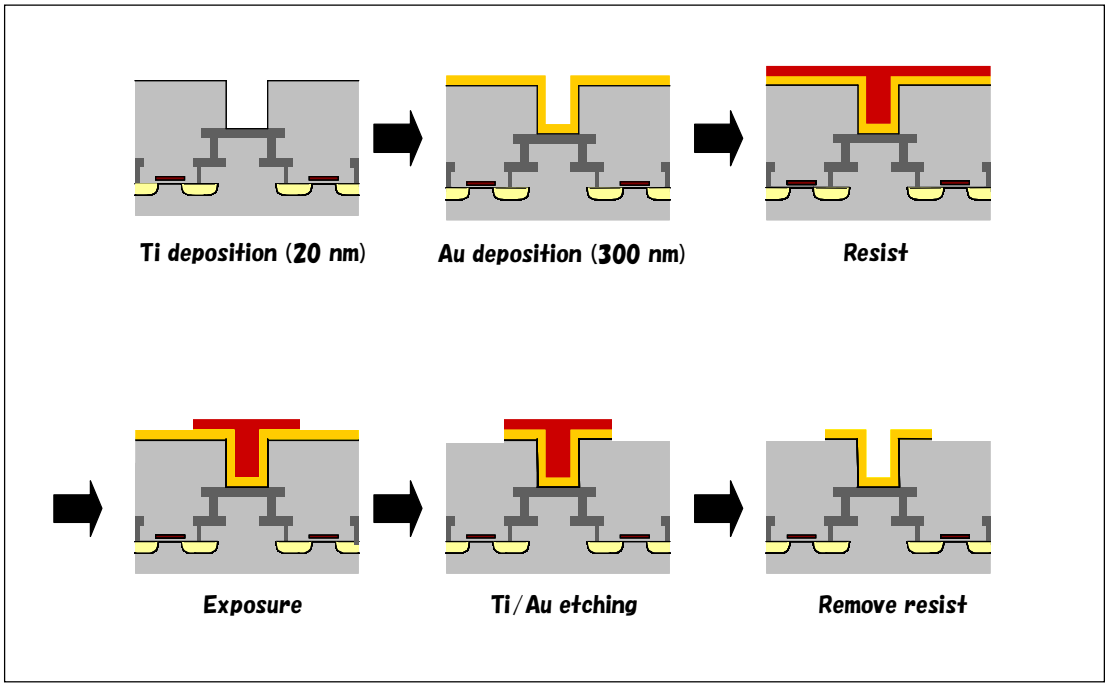

Fig. 3.11 Process flow upon gold electrode preparation.

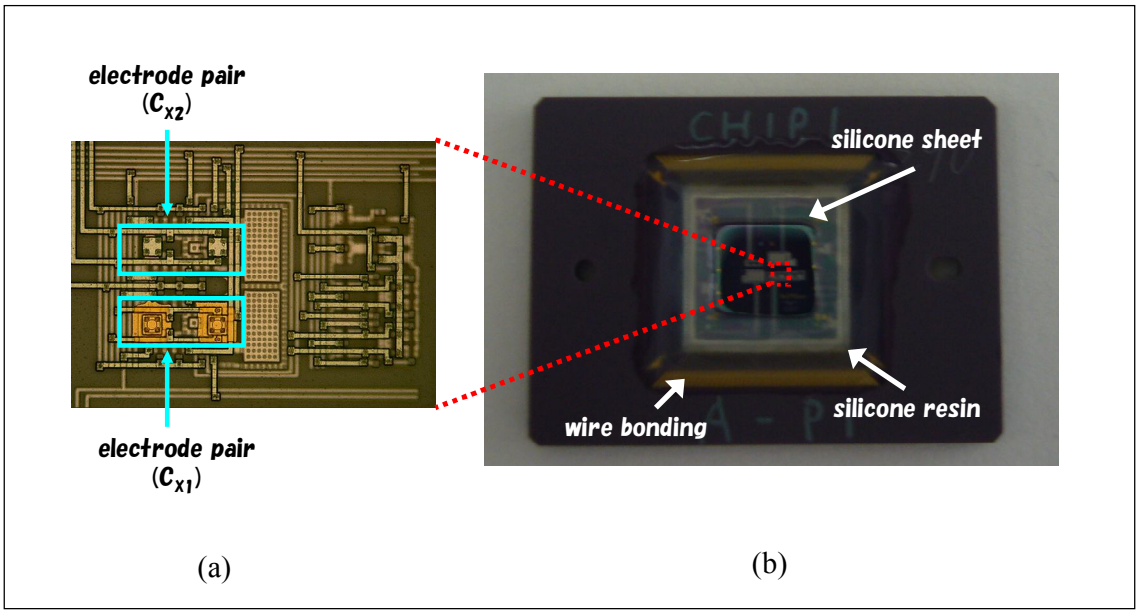

Fig. 3.12 (a) Microphotograph of the electrodes after gold deposition. (b) Electrical isolation of packaged chip before measurement.

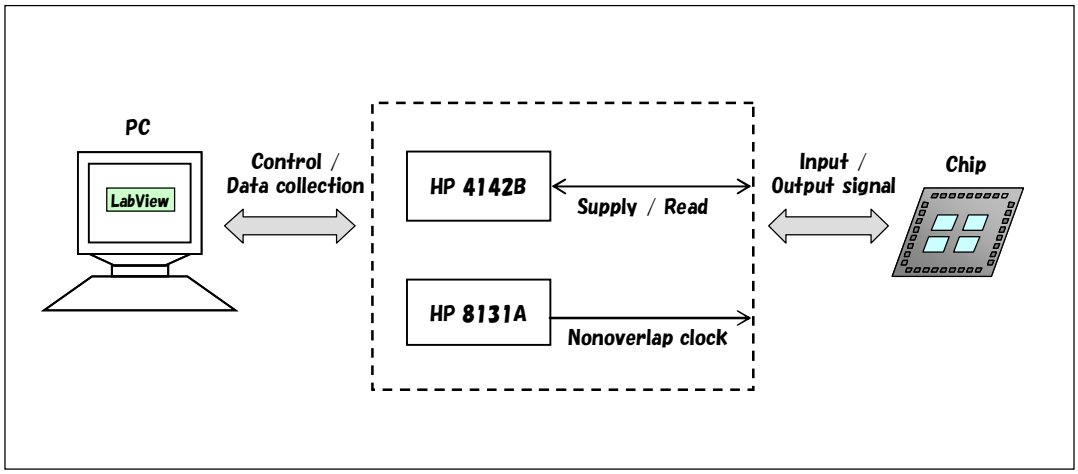

Fig. 3.13 Instrumentation for on-chip capacitance measurement.

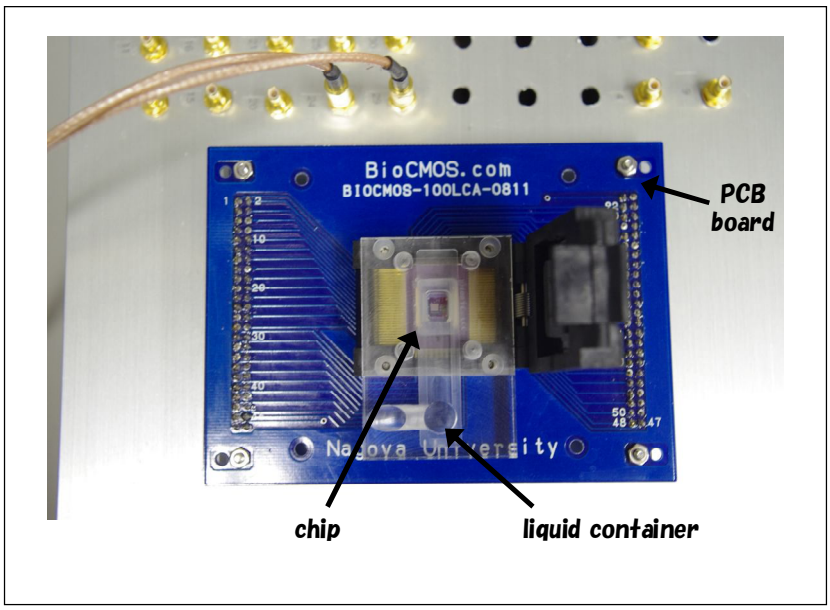

Fig. 3.14 Measurement setup using liquid container.

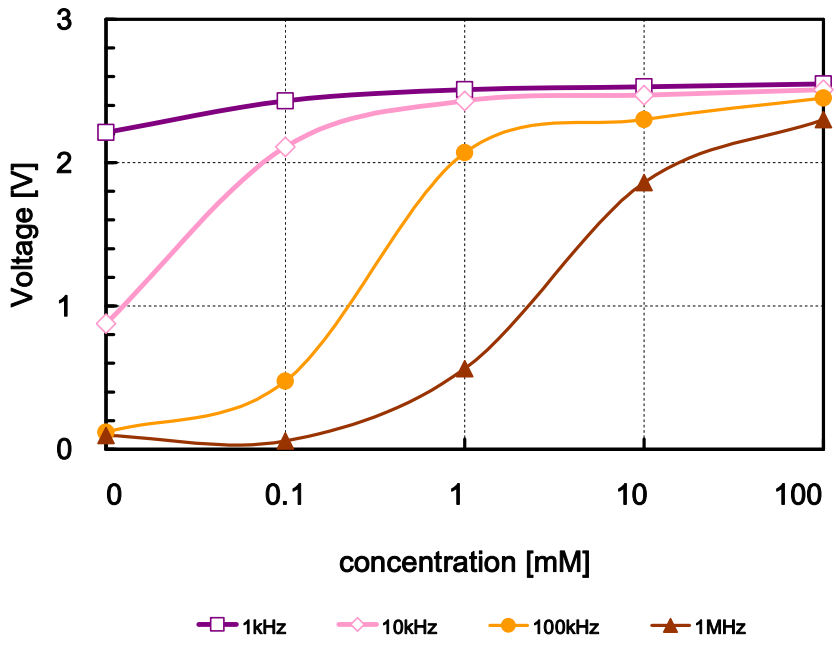

Fig. 3.15 Output voltage against solution concentration for various frequencies.

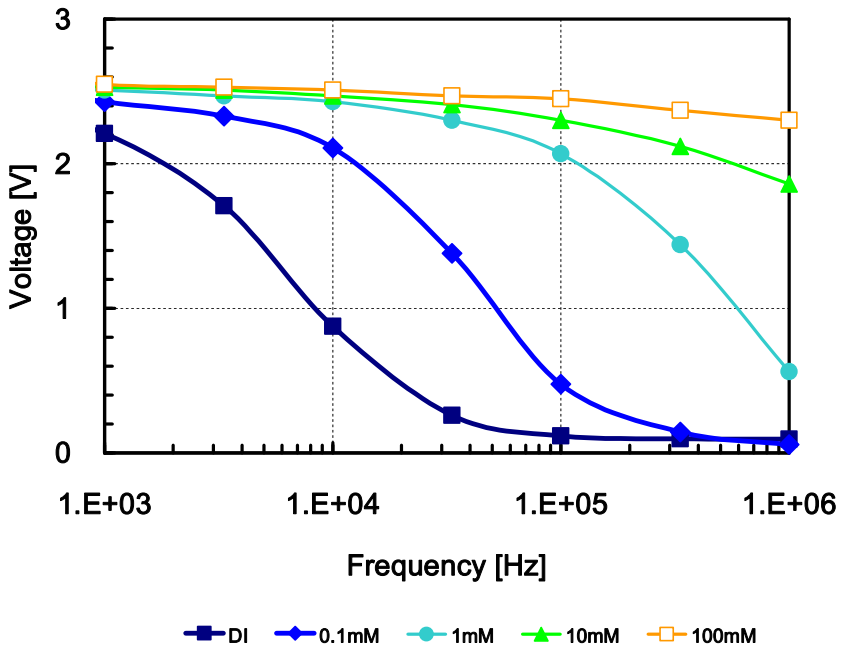

Fig. 3.16 Output voltage against frequency for various concentration of solution.

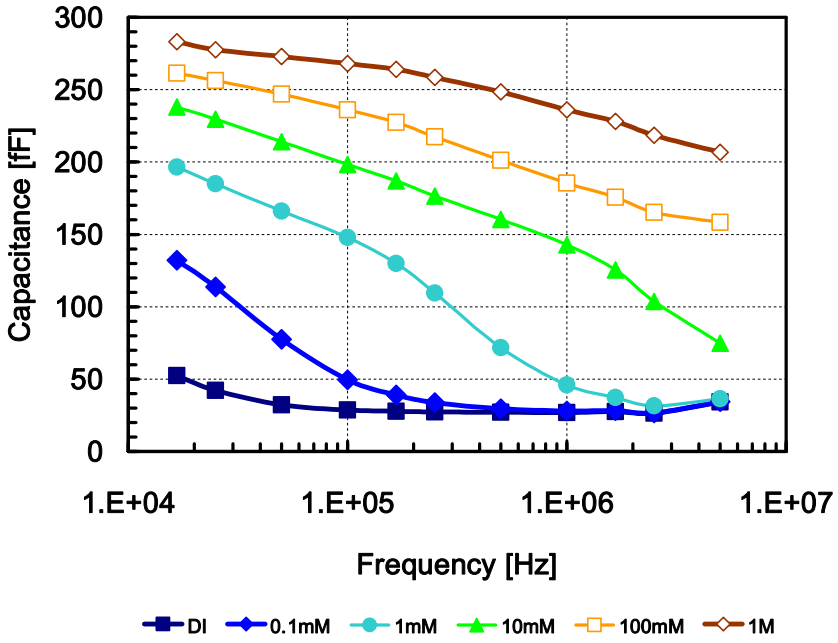

Fig. 3.17 Frequency dependence of capacitance for various concentration of solution.

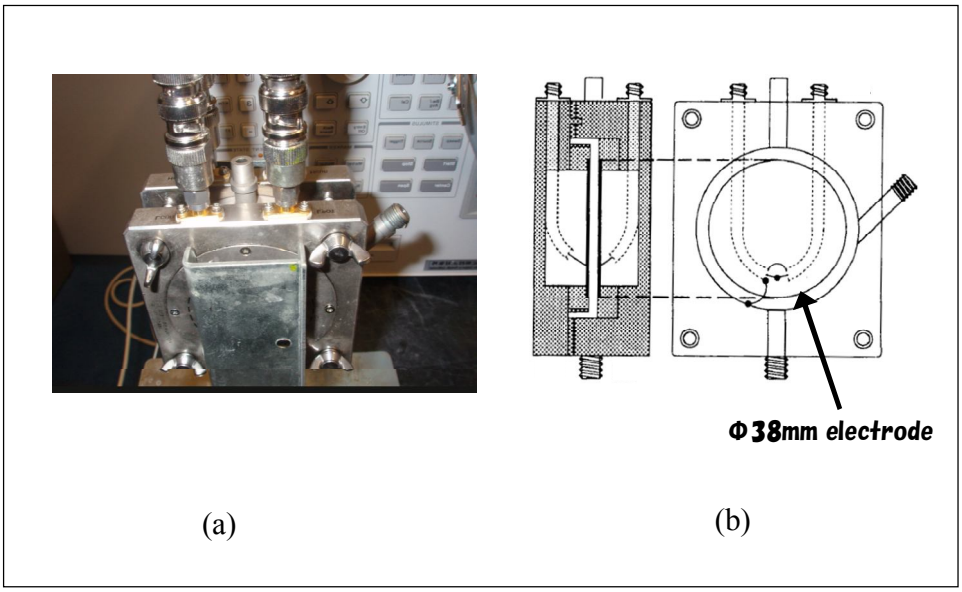

Fig. 3.18 (a) Picture and (b) section view of Agilent 16452A liquid test fixture.

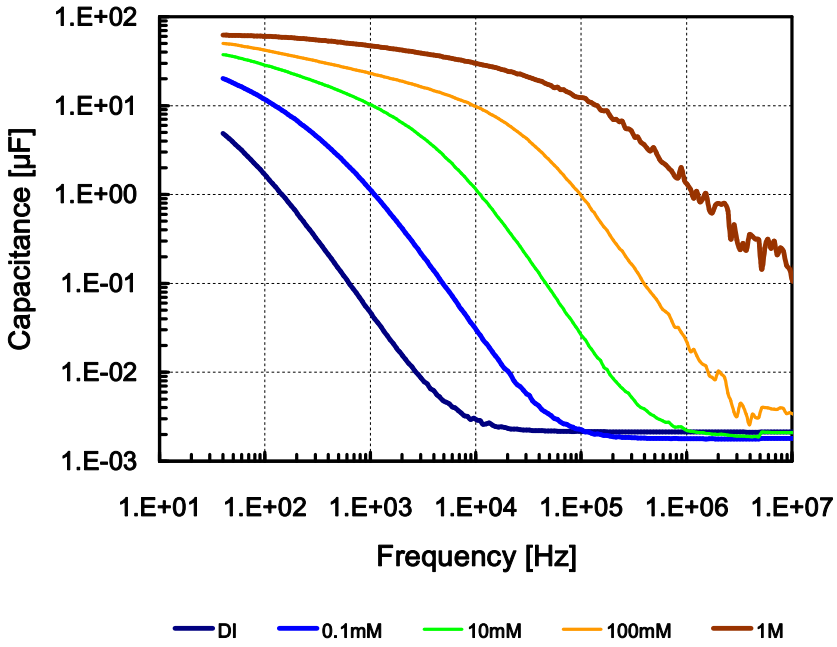

Fig. 3.19 Frequency dependence of capacitance for various concentration of solution using Agilent 16452A liquid test fixture.

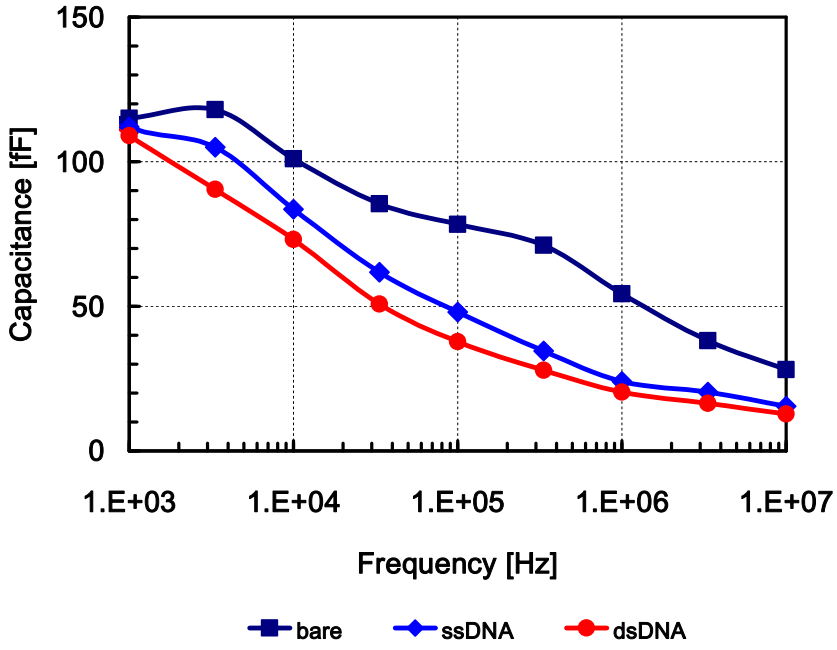

Fig. 3.20 Capacitance against frequency for bare electrode, after single-stranded probe (ssDNA) immobilization, and after double-stranded formation (dsDNA).

Chapter 4

Nonfaradaic EIS of biomodified electrodes

In Chapter 3, a detection of DNA hybridization by monitoring the capacitance variation of the interface has been demonstrated. In this chapter, the event of the DNA hybridization is studied by using electrochemical impedance spectroscopy (EIS) to gain fundamental insight into the associated physical process involved and more precise characterization of the interface. EIS is used to interrogate the charging behavior of the metal-solution interface in response to sinusoidal perturbations in potential of the metal surface.

4.1 Electrochemical impedance spectroscopy

Electrochemical impedance spectroscopy is an impedance technique in which the frequency of a small oscillating perturbing potential at the electrode is varied across a wide range, usually from several tenth of hertz to hundreds of megahertz. The most common way to measure impedance at the electrode surface is by applying a test voltage, V_{test}, which is a constant potential bias (or dc bias) imposed by a small sinusoidal potential perturbation (V_{ac}) of a chosen frequency.

$$V_{\text{test}} = V_{\text{dc}} + V_{\text{ac}} \sin(\omega t) \tag{25}$$

where V_{dc} is the amplitude of the alternating part of the signal and ω denotes its angular frequency (rad s^{-1}). The current response, I_{test} of the system under study is then measured; there is in general a phase shift, θ between I_{test} and V_{test} as indicated in below expression,

$$I_{\text{test}} = I_{\text{dc}} + I_{\text{ac}} \sin(\omega t + \theta) \tag{26}$$

where I_{ac} is the magnitude of the alternating current signal. The relationship between the alternating (or ac) portion of the measured current and the imposed ac potential perturbation according to Ohm's law yields the impedance of the system which is expressed as

$$Z(\omega) = \frac{V_{\text{test}} - V_{\text{dc}}}{I_{\text{test}} - I_{\text{dc}}} . \tag{27}$$

The complex impedance, $Z(\omega)$ has the magnitude of $V_{\text{ac}} / I_{\text{ac}}$ and phase of θ. It depends on both the

dc bias condition and the measurement frequency (ω). The ω-dependence is the basis of impedance spectroscopy, where the process is repeated at different frequencies within a desired range and by doing so allows the investigator to probe physical processes that happen at different characteristic timescales. In other words, EIS technique can effectively separate the elements of the interface process thus giving accurate information on interface parameters. In our particular application, it allows us to obtain the electrical parameters (i.e. capacitance and resistance) of the DNA modified interface.

4.1.1 EIS plots

As mentioned above, the impedance $Z(\omega)$ is in general a complex number and therefore consists of a real part, Z_{Re} and an imaginary part, Z_{Im}:

$$Z(\omega) = Z_{\mathrm{Re}} + jZ_{\mathrm{Im}} \tag{28}$$

where $j = \sqrt{-1}$. Hence, the absolute impedance, $|Z|$ and phase angle, θ can be expressed as

$$|Z| = \sqrt{Z_{\mathrm{Re}}^2 + Z_{\mathrm{Im}}^2} \tag{29}$$

$$\theta = \tan^{-1}\left(Z_{\mathrm{Im}} / Z_{\mathrm{Re}}\right) \tag{30}$$

These data are normally graphed in either a Bode plot or a Nyquist plot (Fig. 4.1). The former is a plot of system response as a function of frequency. It consists of two graphs: the absolute value of the impedance and a phase angle against logarithmic frequency f ($= \omega / 2\pi$). The latter, or also known as a Cole-Cole plot, is a 2D plot of the three variables in eq. (27), where $- Z_{\mathrm{Im}}$ is presented as a function of Z_{Re}, and frequency (f or ω) is an implicit variable. The reason for the negative sign in front of the imaginary part of the impedance is to place the graph in the first quadrant. Nyquist plot is often used in the electrochemical literature because it allow for an easy prediction of the electrical model but does not show all the details of the circuit elements. On the other hand, Bode plots contain all the necessary information and are mainly used in the circuit analysis.

4.1.2 Constant phase element

Impedance of solid electrode usually shows dispersion in their capacitive behavior across a wide frequency range. This can be attributed to microscopic surface roughness [60, 61], local

non-uniformities in current and potential distributions due to chemical inhomogeneities and ion adsorption [62], or both surface and chemical inhomogeneities [63].This non-ideal behavior is best modeled by a circuit element termed a constant phase element (CPE) and denoted by a constant (Q). The impedance due to Q is expressed as

$$Z_{\mathrm{CPE}} = \frac{1}{Q(j\omega)^n} \tag{31}$$

where n is a real number between 0 and 1 such that a value of 1 yields the impedance of an ideal capacitor. Schematic Nyquist plots of a capacitor and a CPE in a single and parallel combination with a resistor are illustrated in Fig. 4.2. When a capacitor is replaced with a CPE, the straight line (shown in red) is tilted to make an angle of (n·90°) with the Z_{Re} axis. In the case of parallel arrangement, the center of the semicircle with diameter R (shown in blue) is depressed by an angle of (1-n)·90° with respect to the Z_{Re} axis.

Generally, the interface impedance is modeled by the parallel combination of a resistor and a capacitor in the equivalent circuit [64]. However, under Warburg`s assumption of a constant phase angle, it may also be modeled by the series combination of a resistor and a capacitor. For parallel combination of R_{p} and C_{p}, the impedance is described as

$$Z_{\mathrm{p}}(\omega) = \frac{R_{\mathrm{p}}}{1+(\omega R_{\mathrm{p}} C_{\mathrm{p}})^2} - j\frac{\omega {R_{\mathrm{p}}}^2 C_{\mathrm{p}}}{1+(\omega R_{\mathrm{p}} C_{\mathrm{p}})^2}. \tag{32}$$

For the series combination of R_{w} and C_{w}, the impedance is

$$Z_{\mathrm{w}}(\omega) = R_{\mathrm{w}} - j\frac{1}{\omega C_{\mathrm{w}}}. \tag{33}$$

Both models are intended to represent the same physical system and thus $Z_{\mathrm{p}} = Z_{\mathrm{w}}$. This equality yields

$$R_{\mathrm{p}} = R_{\mathrm{w}}\left(1+\frac{1}{(\omega R_{\mathrm{w}} C_{\mathrm{w}})^2}\right), \tag{34}$$

$$C_{\mathrm{p}} = \frac{C_{\mathrm{w}}}{1+(\omega R_{\mathrm{w}} C_{\mathrm{w}})^2}. \tag{35}$$

Warburg stated that at low current densities both R_{w} and C_{w} vary as the square root of frequency, $1/\sqrt{\omega}$. The consequence of this relationship is that the phase angle, which equals to $\tan^{-1}(\omega R_{\mathrm{w}} C_{\mathrm{w}})$ is constant at 45° at all frequencies. For the special case $\omega R_{\mathrm{w}} C_{\mathrm{w}} = 1$, the above

relations become

$$R_{\mathrm{p}} = 2R_{\mathrm{w}}\,, \tag{36}$$

$$C_{\mathrm{p}} = \frac{C_{\mathrm{w}}}{2}\,. \tag{37}$$

This indicates that parallel and series circuits, become equivalent under Warburg's assumption, and the conversion from one circuit to the other is a simple factor of 2. However, the series representation of interface does not allow the passage of the direct current, and as ω approaches zero, the condition $\omega R_{\mathrm{w}} C_{\mathrm{w}} = 1$ breaks down. Thus, at low frequencies, the parallel model is more appropriate than the series model and most commonly used to describe the interface impedance.

4.2 Experimental

4.2.1 Electrode preparation

Noble metals are known to create strong affinity bonds with chemical compounds terminating with a thiol (-SH) group. Since the common way of attaching DNA molecules to the solid surface is via the use of thiol linker, gold deposition is performed at the electrode surface, which the substrate is made from an aluminium alloy and has a diameter of 20 mm. Prior to the deposition, the substrate is polished with 2000-grid sandpaper, followed by 0.1 and 0.05 μm alumina slurry on microcloth pads until mirrored surface is obtained. Then, it is cleaned by sequential ultrasonic bathing for 5 min each in ethanol, acetone, isopropanol, and DI water. 20 nm layer of titanium (Ti) coating is first carried out, followed by a 300 nm layer of gold (Au) using thermal vapor deposition in a vacuum chamber. The gold electrodes are stored in a vacuum desiccator until use.

4.2.2 Liquid test fixture

The liquid test fixture with disposable electrodes feature is designed and fabricated, as shown in Fig. 4.3. The effect of the stray capacitance due to edges of the electrodes is minimized by built-in approach. The use of acrylic as liquid container's material also reduces the contribution of stray capacitance to the measurements since it has low dielectric constant (ε_{r}=3.3) compared to water

(ε_r=78). Two gold electrodes are placed face-to-face and separated by distance keepers (1 mm) located at the container's cap. After the cap is sealed with paraffin tape, the measurement solution is injected through the inlet at the top. The container is filled until excess liquid flows out from the outlet. Each of the electrodes is electrically connected by a pair of coaxial cables to four contact terminals located at the metal case of the test fixture.

4.2.3 Impedance measurement

All impedance measurements are carried out at room temperature. As shown in Fig. 4.4, contact terminals of the test fixture are connected by 1-m-length 16048G cable to the input of an Agilent 4294A precision impedance analyzer. Open circuit calibration is performed to remove parasitics due to the instrumentation and cables. Measurements are done in the frequency range from 40 Hz to 110 MHz. In order not to disturb the probe layer which their covalent bond energies are about 1-3 eV, a small modulation voltage of 25 mV in amplitude and a dc bias of zero is applied. Bandwidth is chosen to 5 (most precise) and 500 measurement points are taken in a logarithmic scale. Before every measurement, nitrogen gas bubbling is performed to each solution in order to reduce the measurement drift due to the penetration of air vapor into the solution. All solutions contain no electroactive species and are freshly prepared prior to the measurement.

4.2.4 Chemicals and biomaterials

All chemicals are purchased from Kanto Chemical, Japan. NaCl aqueous solutions of five different concentrations from 0.1 mM to 1 M are prepared. The phosphate-buffered saline (PBS) is pH 7.0 and contains 0.1 M KH_2PO_4, 0.1 M K_2HPO_4, 0.1 M NaCl, and 1 mM ethylene-diamine -tetraacetic acid (EDTA). All solutions are prepared with deionized (DI) water (18 MΩ cm, Millipore). Mercaptohexanol ($SH(CH_2)_6OH$, 97%) is purchased from Sigma Aldrich, Japan. The DNA used in this study is purchased from Hokkaido System Science, Japan. The thiol-modified single-stranded DNA (probe DNA) is a 20-mer oligonucleotide with the sequence 5'-HS-$(CH_2)_6$-GGGAAAAAAAAAAAAAGGG-3'. The probes are provided in the protected form with the disulfide linkage intact and dithiothreitol is used to free the probes. The probes is then

diluted with PBS and filtered by passing them through a NAP-10 column. The complementary single-stranded DNA (target DNA) is a 20-mer oligonucleotide with the sequence 5'-CCCTTTTTTTTTTTTTTCCC-3'. For the control of the nonspecific response of the functionalized gold electrode, measurements are performed using the noncomplementary oligonucleotides (control DNA), which has the same sequence as the probe DNA without the thiol ($HS-(CH_2)_6-$) attachment at the 5' end terminus.

4.2.5 Surface modification

For modification of alkanethiol self-assembled monolayer on gold, direct immersion approach is used. The fresh electrode is placed in a 1 μM aqueous solution of mercaptohexanol (MCH) for 4 hours, then rinsed with DI water twice, and dried by nitrogen gas blowing.

Schematic process of DNA modification onto gold electrodes is illustrated in Fig. 4.5. Immobilization of capture probe DNA is carried out using a self-assembly method, which exploited the strong sulfur-gold interactions between the SH headgroups of DNA linker molecules and the gold substrate [65]. Two electrodes are immersed in a PBS containing 1 μM 20-mer thiol-modified probe DNA. After 4 hours of immersion at room temperature, the electrodes are rinsed twice with the PBS to remove unattached probes. One of the electrodes is subsequently immersed in a 1 μM MCH aqueous solution for 2 hours, before again being rinsed with DI water and PBS twice. Complementary hybridization is conducted by spreading the dissolved 20-mer target DNA at a concentration of 1 μM in PBS onto the probe-modified electrodes and heated up to 70°C for at least 30 minutes. After cooled down to room temperature, the electrodes are incubated for one hour to allow hybridization, and then rinsed thoroughly in PBS twice. For noncomplementary hybridization measurement, the control DNA diluted in PBS is treated in the same condition as complementary hybridization for comparison.

4.3 Results and discussions

4.3.1 System characterization

Bode plots (absolute impedance and phase) and Nyquist plots measured for bare gold electrodes in aqueous solutions with different concentrations are shown in Fig. 4.6 and 4.7, respectively. At high frequencies, the impedance of bulk solution is dominant. It can be observed in Fig. 4.6 that the resistance (magnitude of horizontal line which its phase approaches zero) decreases as concentration increases and solution capacitance (slope=-1 with the phase drops to -90°) is constant at all conditions with the measured average value of 2.57×10^{-10} F (theory $=2.24\times10^{-10}$ F at room temperature). The first complete semicircle in Nyquist plot (Fig. 4.7) indicates that this impedance can be expressed as a parallel combination of solution resistance (R_S) and solution capacitance (C_S). On the other hand, the interfacial impedance dominates at low frequencies and the second incomplete semicircle (Fig. 4.7) indicating that the low-frequency impedance is mainly capacitive. However, the phase of the impedance at low frequencies drops below zero (Fig. 4.6(b)) is not approaching -90° (in case of a capacitor), thereby the impedance should represented by a constant phase element (CPE) and can be modeled with the parallel combination of a resistor and a capacitor (refer Section. 4.1.2). All these four elements describe the system as represented in Fig. 4.8. The equivalent circuit can be interpreted essentially as follows; the solution capacitance C_S in parallel with the solution resistance R_S for electrolyte solution dominated at high frequencies, and double layer capacitance C_{dl} in parallel with the polarization resistance R_p for interfacial impedance dominated at low frequencies. The equation expression is

$$\begin{aligned} Z(\omega) &= \frac{R_S}{1+j\omega R_S C_S} + \frac{R_p}{1+j\omega R_p C_{dl}} \\ &= \frac{R_S}{1+(\omega R_S C_S)^2} + \frac{R_p}{1+(\omega R_p C_{dl})^2} - j\omega\left(\frac{{R_S}^2 C_S}{1+(\omega R_S C_S)^2} + \frac{{R_p}^2 C_{dl}}{1+(\omega R_p C_{dl})^2}\right) \\ &= Z'(\omega) + jZ''(\omega) \end{aligned} \tag{38}$$

where ω represents the angular frequency.

4.3.2 MCH modified electrode

As previously discussed in Sec. 3.1.3, the electrical double layer arising from electrode polarization will change when the electrode surface experience a chemical or biological modification. To observe this change, a measurement using self-assembled monolayer (SAM) of mercaptohexanol (MCH) is performed. A significant change in impedance spectra of the gold electrode upon

formation of MCH monolayer is observed. It is clearly visible that the impedance curve in the bode plot is shifted upwards for frequencies below 10 kHz (Fig. 4.9) and imaginary impedance in the Nyquist plot is about two times higher than the bare electrode (Fig. 4.10). The capacitance of C_{dl} in Fig. 4.8 is now can be substituted with interfacial capacitance, C_{INT} that is a total of series capacitances of SAM layer and C_{dl} (eq. (14)). C_{INT} and R_p at each frequency can be determined as

$$C_{INT}(\omega) = -\frac{Z''}{\omega\left\{(Z'-R_S)^2 + Z''^2\right\}} \quad , \tag{38}$$

$$R_p(\omega) = \frac{Z''^2 + (Z'-R_S)^2}{Z'-R_S} \quad . \tag{39}$$

where, the solution resistance R_S is 2.13 Ω (value read from the Nyquis plot where the curve intersect the horizontal axis). The extracted C_{INT} and R_p are plotted in Fig. 4.11 (a) and (b), respectively. A substantial decrease in C_{INT} can be seen after the formation of MCH. This is expected since the use of SAM on electrode diminishes double layer effects (ε_{MCH}~2.7<ε_{water}) and minimizes charging current, inferring decreases capacitance. It can be observed that the resistance is also a frequency dependent. In contrast to the behavior of C_{INT}, the increase in the resistance only visible for frequencies below 300 Hz after MCH formation. The increase in R_p should be due to the blocking behavior of the SAM, where the closely packed structure hinders the approach of ions from solution to the electrode surface. At high frequencies, R_p becomes zero when R_S is effective instead of R_p.

4.3.3 DNA hybridization

DNA hybridization is demonstrated using 20-mer thiol-modified single-stranded DNA (probe) and its complementary single-stranded DNA (target) with the same length. The measured impedance in Bode plot showed that immobilization with probe DNA yielded an about two-fold increase compared to those of the bare electrode for frequencies below 10 kHz (Fig. 4.12). This is expected as the thiol linkers used at the 5'end of DNA oligonucleotides formed a dielectric SAM and the attached DNA molecules further increase the layer thickness thus increases the total interface impedance. Hybridization of target DNA to the capture probe caused a positive shift in impedance but the behavior is somewhat different as the change becomes smaller at frequencies under several

hundreds hertz. This phenomenon is expected to be related to the DNA layer behavior. Better view of this impedance change at low frequency can be observed from the Nyquist plot (Fig. 4.13). It can be observed that the angle of the curve is slightly tilted towards the horizontal axis after the hybridization. This may suggest that a second CPE element is appeared in series with the CPE element of SAM and a more complex model may be considered to describe the interface. The increase of the imaginary impedance is significant in target hybridization than its noncomplementary (control), confirming binding selectively of the surface-attached probe DNA. The decrease in the interface capacitance of maximum 40% at high frequencies (>1 kHz) to minimum 12% at the lowest frequency is observed for the hybridized electrode (Fig. 4.14 (a)). According to literatures [66-68], hybridization causes the ion displacement due to the increased negative charges at DNA molecules, thus increasing the distance of the charge inside the electrode and the ion layering in the solution (i.e. effective layer thickness), which implies a decreased in capacitance. However, a slight decrease in resistance is also registered after the target hybridization for frequencies below 1 kHz (Fig. 4.14(b)). This is surprising considering the assumption that formation of double stranded DNA will increase the layer thickness (i.e. ion displacement, physical thickness (see Sec. 3.1.3), etc) or doubles the negative charges (as DNA carries negative charge on its phosphate backbone) thus expected to introduce higher barrier for the electrolyte ions in their approach to the electrode. Therefore, the result of a decrease in resistance after specific hybridization inferring that there is an increase in ion accessibility to the electrode. Then, it comes to the question whether the formation of single-stranded DNA to double-stranded DNAs would cause some defects (e.g. pinholes, collapsed sites, etc.) in the monolayer. It was thought that the thiol group at the single end of DNA molecules formed a densely packed SAM structure and allowed no ions for passing through, but the fact that DNA carries negative charges on its backbone would affect the neighboring probes to be separated at a certain distance due to the electrostatic repulsion between them during immobilization. Since the diameter of a DNA duplex is about 2.4 nm [69], the distance between the DNAs is expected to be at least 5 nm. These open space or pinholes would allow electrolyte ion that has an ionic radius on the order of 0.1 nm to reach the electrode surface. Collapsed sites would be due to the nonspecifically binding of probe DNA through the nucleotide bases to the electrode surface that will allow a closer ion approach than that expected for a full thickness probe layer.

To address this problem, another experiment is conducted where a diluent SAM of alkanethiol is

used to fill the empty space and at the same time can remove the nonspecific adsorption of the probe DNA off the gold surface. A diluent of mercaptohexanol (MCH) is employed because its length is similar to the length of the linker (C6) of the probe DNA used in this experiment, which enables high hybridization efficiency (90%) [70]. A Bode plot of a hybridized electrode shows no obvious change in impedance, except for the frequencies below several hundreds hertz (Fig. 4.15). However, a considerable change of the impedance curve before and after target hybridization can be observed at the corresponding Nyquist plot (Fig. 4.16), confirming the occurrence of specific hybridization at the electrode surface. In contrast to the result in Fig. 4.14(a), the increase in capacitance is found after hybridization at low frequencies below 200 Hz with no significant change for the rest of the frequencies (>200 Hz), as shown in Fig. 4.17(a). A visible decrease in resistance can be seen after the target hybridization for frequencies below 1 kHz (Fig. 4.17(b)). By assuming the modified probe layer backfilled with MCH could restrain the effect of defects, these observations give a hint that the impedance change is due to the DNA itself. In particular, two reasons can be considered; a change in physical properties of the DNA upon transformation from single-stranded to double-stranded structure and/or a change in electrical properties of the DNA itself. Regarding the former, there are observations in several literatures that single-stranded DNA is floppy and prone to lying near the surface and hybridization will transform it into a rigid rod of DNA duplex causing an ion gating effect [71-73]. This can explain our results; hybridization causes DNA to stand up from the lying down position on a diluent SAM and open the space for ions to get closer to the electrode, thus increase the ion accessibility (decrease in resistance) and decrease the thickness of the layer (increase in capacitance) as illustrated in Fig. 4.18. The latter can be due to the increase of charge transfer in DNA as hybridization doubles the negative charges of the DNA strands resulted in more efficient electron transfer [74-76]. Since our approach does not involve any electroactive species for electron change to and from the electrode surface, and any additional bias for pulling DNA probes to stand straight and parallel to each other in order to form a well organized monolayer, it's difficult to consider this as a reason. Nevertheless, it awaits further investigation in the future to clarify the electronic properties change contribution to the impedance variation.

4.4 Support measurement

To support the hypothesis discussed above, an alternative approach for simple investigation of the ion accessibility upon DNA hybridization is considered.

4.4.1 Cyclic voltammetry

Cyclic voltammetry (CV) is one of the conventional electrochemical measurement methods that can provide information on transient (charging) current of the double layer structure. The main components to perform CV are the reference electrode, auxiliary electrode, working electrode and potentiostat. The potentiostat is an instrument that controls the potential of the working electrode with respect to the reference electrode while also measuring the current flow between the working electrode and auxiliary electrode. In CV, the potential of a working electrode is cycled linearly (forward and backward) between two values at a fixed rate and the current response is measured throughout. The resulting current-potential curve is called a cyclic voltammogram. Fig. 4.19 shows a typical CV curve, where the peak current is apparent in the use of a reducible redox complex.

4.4.2 Measurement and result

Cyclic voltammetry is performed in PBS without any redox species. The measurement is performed with an ALS/CHI610D electrochemical analysis (BAS Inc.). The potential is scanned between -200 mV and 600 mV in reference to the Ag/AgCl, saturated KCl electrode at scan rate of 100 mV/s and a platinum wire is used as an auxiliary electrode. Cyclic voltammograms of gold electrodes after probe/MCH immobilization and after the specific hybridization is shown in Fig. 4.20. The beginning of gold oxidation at approximately 500 mV vs. Ag/AgCl can be observed and both voltammograms exhibit no significant difference in shape except for a small broadening of nonfaradaic current after target hybridization. Since this nonfaradaic current is due to resulted interfacial layer (capacitor) in an inert electrolyte, the increase in current represents larger capacitance, which might suggest a nearer ion layering to electrode and decreased interfacial layer thickness. This result is consistent with the hypothesis that a flexible single-stranded DNA

transforms into a rigid rod upon hybridization, which causes DNA to stand up from the lying down position on the surface and thereby open the space for ions to get closer to the electrode (Fig. 4.18).

4.5 Conclusions

In this work, impedance change of biochemically modified gold electrode in a solution is investigated using a nonfaradaic electrochemical impedance spectroscopy. Two surfaces of probe capture layer are measured; thiol-modified single-stranded DNAs and thiol-modified single-stranded DNAs with MCH backfilling. In both measurements, the increase in interface impedance after complementary target hybridization is observed. Further analysis of interface capacitance and resistance has found that this impedance change is probably due to the physical changes of DNA molecules: a flexible single-stranded DNA transforms into a rigid rod upon binding, causes it to stand up off the surface and opening a space for ions to access to the electrode. The assumption of the increase in layer thickness (or decrease in capacitance) due to ion displacement upon hybridization is not valid if the decrease in resistance is too high in which the capacitance might also increase as ions could come closer to the electrode surface. In other words, it can be said that DNA hybridization should increase the impedance but not limited to a decrease in capacitance. As a conclusion, it is suggested that the impedance change upon DNA hybridization is due to the physical changes of DNA molecules resulting in the variation of electrical double layer thickness and ion accessibility.

[**References**]

60. R. D. Levie, *On impedance measurements: The determination of the double layer capacitance in the presence of an electrode reaction.* Electrochim. Acta, 1965, 10, 4, pp. 395-402.
61. S. H. Liu, *Fractal model for the ac response of a rough interface.* Phys. Rev. Lett., 1985, 55, pp. 529-532.
62. T. Pajkossy, *Impedance of rough capacitive electrodes.* Electroanal. Chem., 1994, 364, pp. 111-125.
63. Z. Kerner, T. Pajkossy, *On the origin of capacitance dispersion of rough electrodes*. Electochim.

Acta, 2000, 46, pp. 207-211.

64. J. B. Jorcin, M. Orazem, et al., *CPE analysis by local electrochemical impedance spectroscopy.* Electrochim. Acta, 2006, 51, pp. 1473-1479.
65. T. M. Herne, M. J. Tarlov, *Characterisation of DNA probes immobilized on gold surfaces.* J. Am. Chem. Soc., 1997, 119, 38, 8916-8920.
66. C. Berggren, P. Stalhandske, J. Brundell, G. Johansson, A feasibility study of a capacitive biosensor for direct detection of DNA hybridization. Electroanalysis, 1999, 11, pp. 156-160.
67. C. Guiducci, C. Stagni, A. Fischetti, U. Mastromatteo, B. Ricco, *Microelectrodes on a silicon chip for label-free capacitive DNA sensing.* IEEE Sens. J., 2006, 6, 5, pp. 1084-1093.
68. S. Carrara, F. K. Gurkaynak, C. Guiducci, C. Stagni, L. Benini, Y. Leblebici, B. Samori, G. D. Micheli, *Interface layering phenomena in capacitance detection of DNA with biochips*. Sens. Transducer J., 2007, 76, pp. 969-977.
69. R. E. Dickerson, H. R. Drew, B. N. Conner, M. L. Kopka, P. E. Pjura, *Helix geometry and hydration in A-DNA, B-DNA, and Z-DNA*. Cold Spring Harbor symp. Quant. Biol., 1983, 47, pp. 13-24.
70. E. L. S. Wong, E. Chow, J. J. Gooding, *DNA recognition interfaces: the influence of interfacial design on the efficiency and kinetics of hybridization*. Langmuir, 2005, 21, pp. 6957-6965.
71. J. J. Gooding, A. Chou, F. J. Mearns, E. L. S. wong, K. L. Jericho, *The ion gating effect: using a change in flexibility to allow label free electrochemical detection of DNA hybridization.* Chem. Commun., 2003, pp. 1938-1939.
72. A. Poghossian, A. Cherstvy, S. Ingebrandt, A. Offenhausser, M. J. Schoning, *Possibilities and limitations of label-free detection of DNA hybridization with field-effect based devices.* Sens. Actuators B, 2005, 111-112, pp. 470-480.
73. F. J. Mearns, E. L. S. Wong, K. Short, D. B. Hibbert, J. J. Gooding, *DNA biosensor concepts based on a change in the DNA persistence length upon hybridization.* Electroanalysis, 2006, 18, pp. 1971-1981.
74. R. E. Holmlin, P. J. Dandliker, J. K. Barton, *Charge transfer through the DNA base stack.* Angew. Chem. Int. Ed., 1997, 36, pp. 2714-2730.
75. J. Jortner, M. Bixon, T. Langenbacher, M. E. Michel-Beyerle, *Charge transfer and transport in DNA*. Proc. Natl. Acad. Sci. USA, 1998, 95, pp. 12759-12765.

76. P. Aichi, S. L. Labiuk, L. W. Tari et al., *M-DNA: a complex between divalent metal ions and DNA which behaves as a molecular wire*. J. Mol. Biol., 1999, 294, pp. 477-485.

4.6 Figures

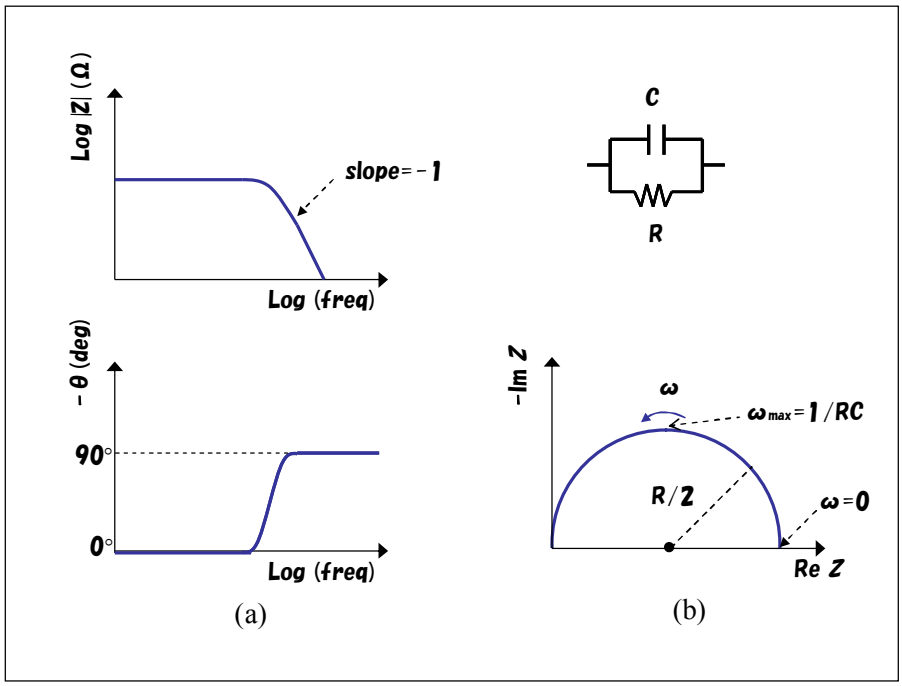

Fig. 4.1 (a) Bode and (b) Nyquist plots for a parallel connection of R and C.

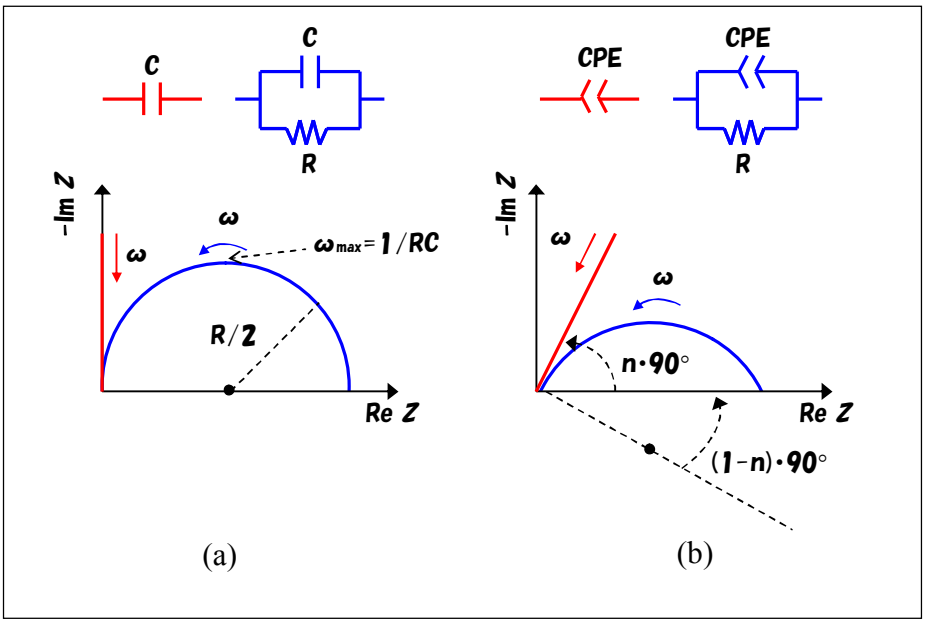

Fig. 4.2 A schematic Nyquist plot of (a) a capacitor and a parallel combination of a resistor and a capacitor, and (b) a CPE and a parallel combination of CPE and a resistor.

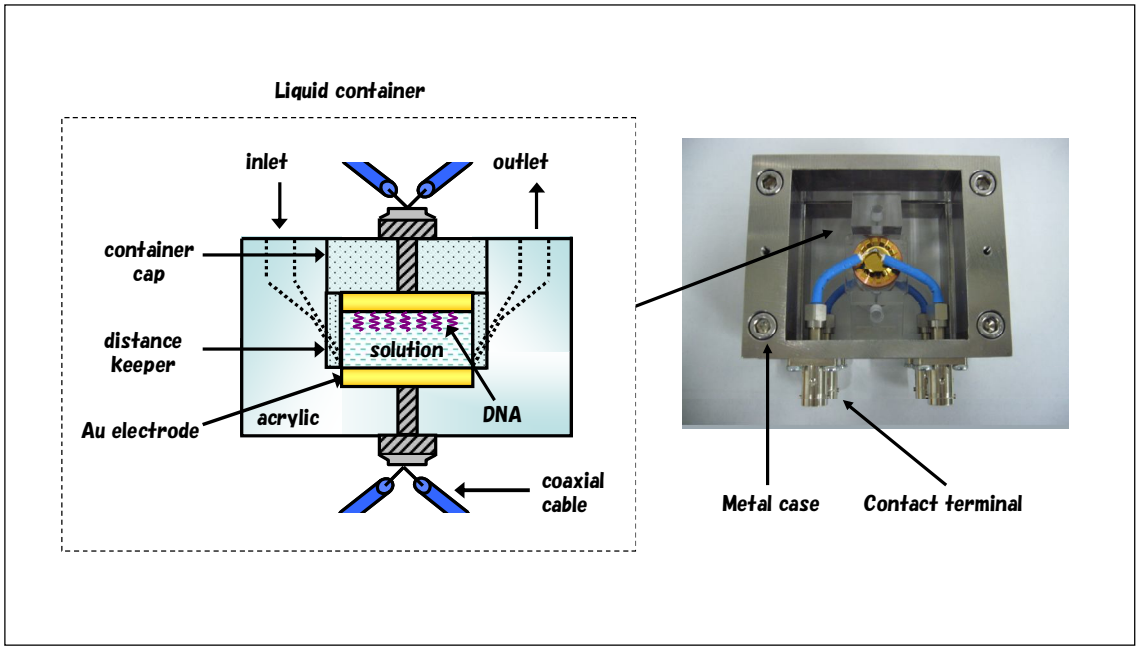

Fig. 4.3 Liquid test fixture and a cross view of the liquid container.

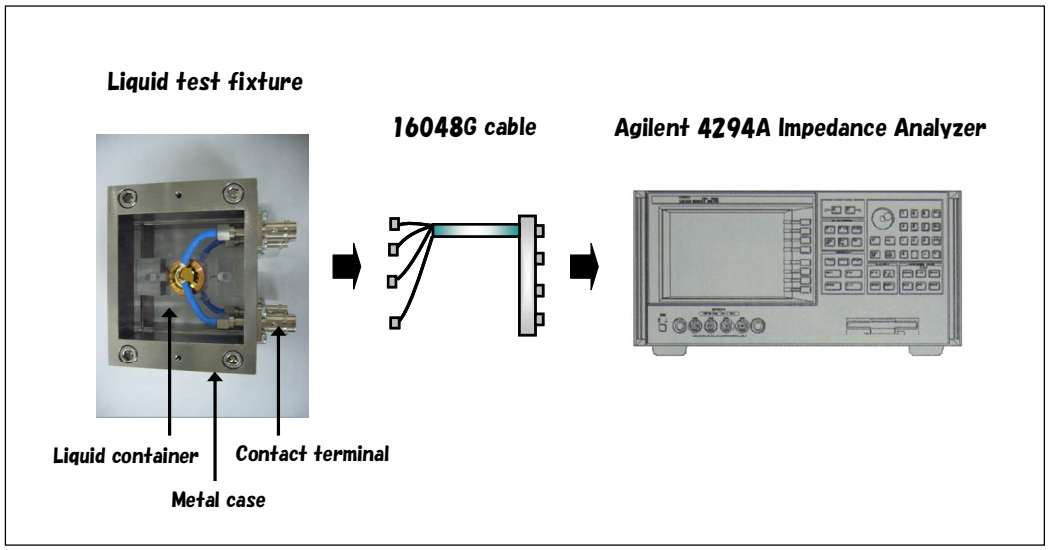

Fig. 4.4 Measurement setup using a liquid test fixture connected to impedance analyzer by a 1-m-length cable.

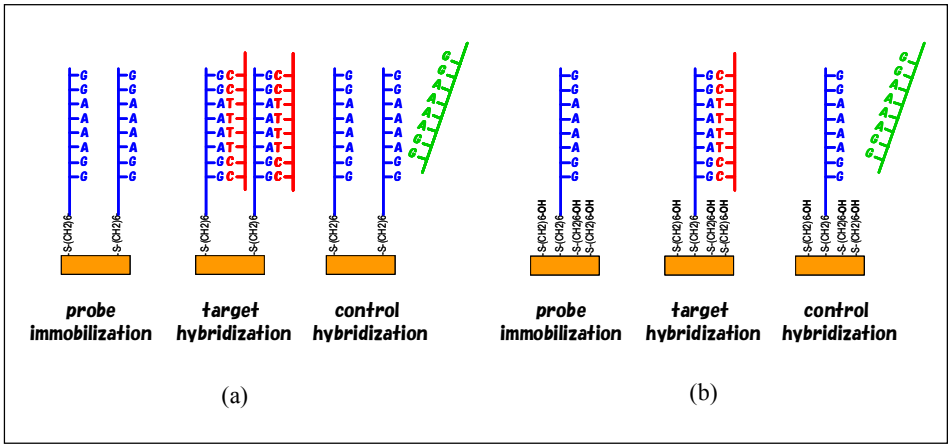

Fig. 4.5 DNA measurements using (a) probe modified electrode, and (b) probe/MCH modified electrode.

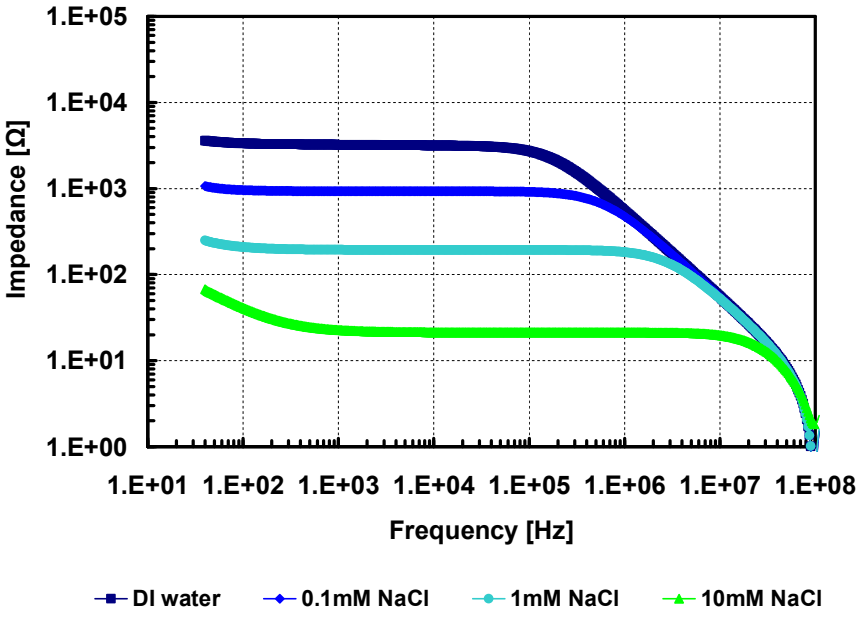

(a)

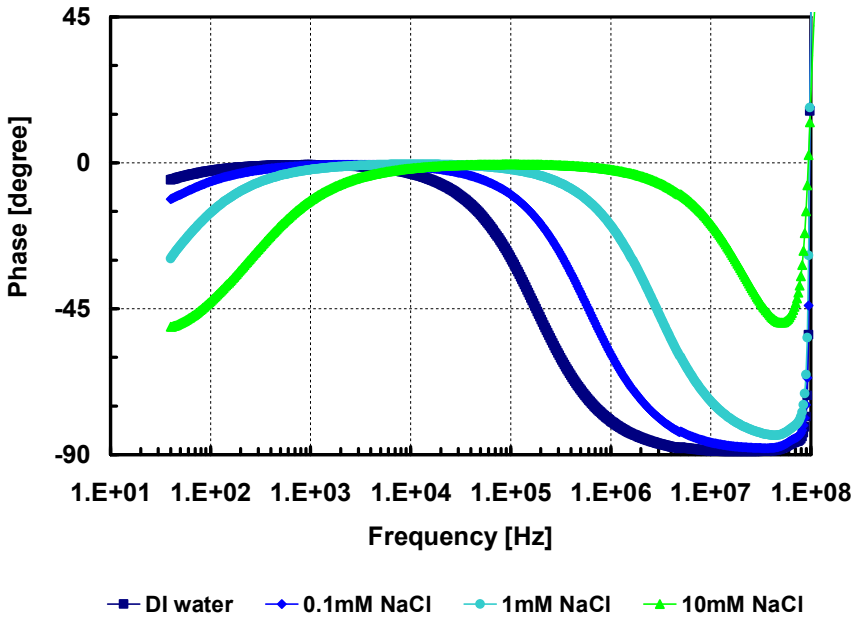

(b)

Fig. 4.6 Bode plot of bare electrode in various solutions. (a) Impedance against frequency. (b) Phase against frequency.

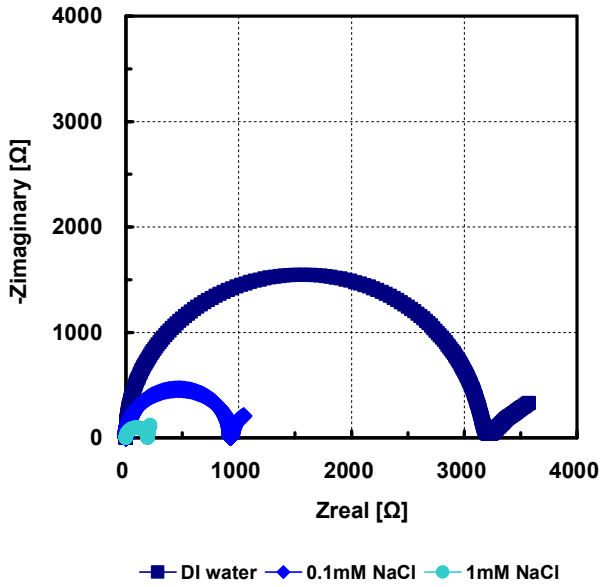

Fig. 4.7 Nyquist plot of bare electrode in various solutions.

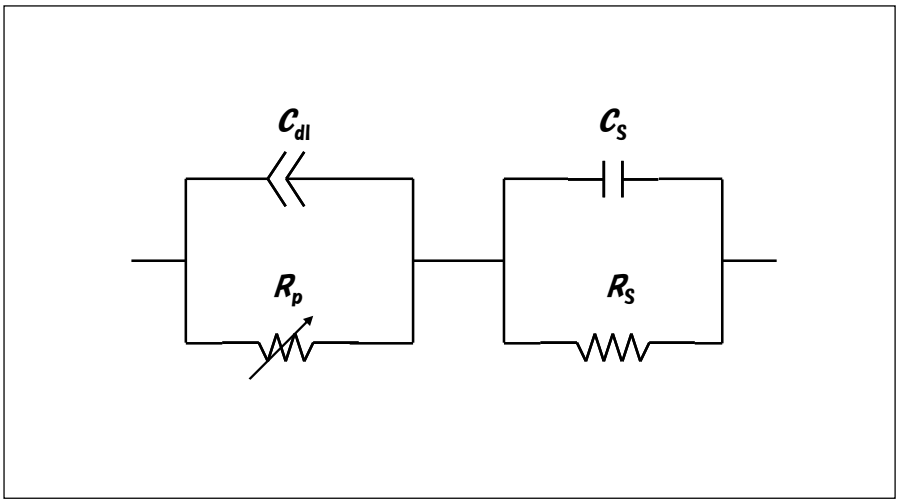

Fig. 4.8 Equivalent circuit model consists of four elements; solution resistance (R_S), solution capacitance (C_S), polarization resistance (R_p), and double layer capacitance (C_{dl}).

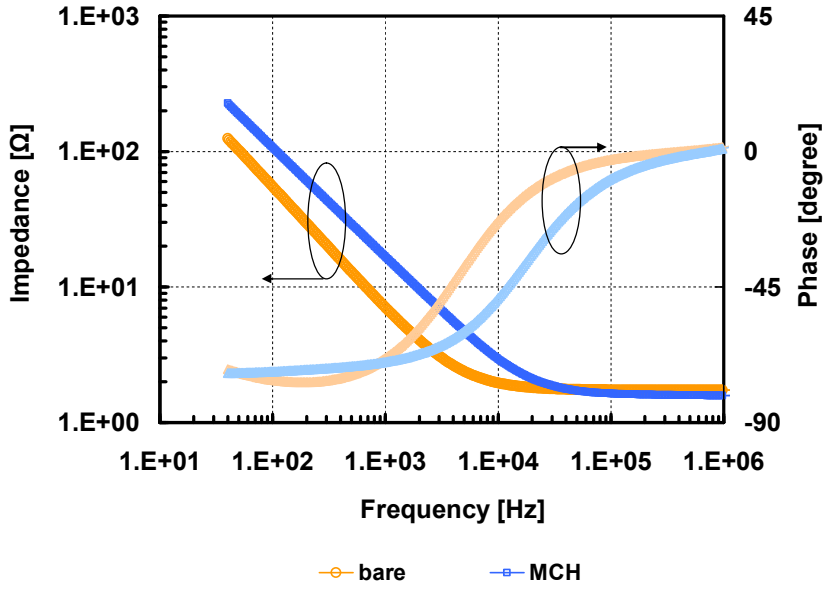

Fig. 4.9 Bode plot of MCH-modified electrode in buffer solution.

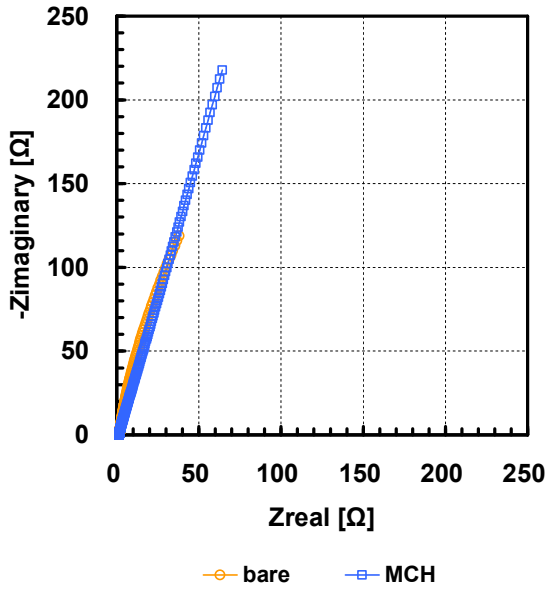

Fig. 4.10 Nyquist plot of MCH-modified electrode in buffer solution.

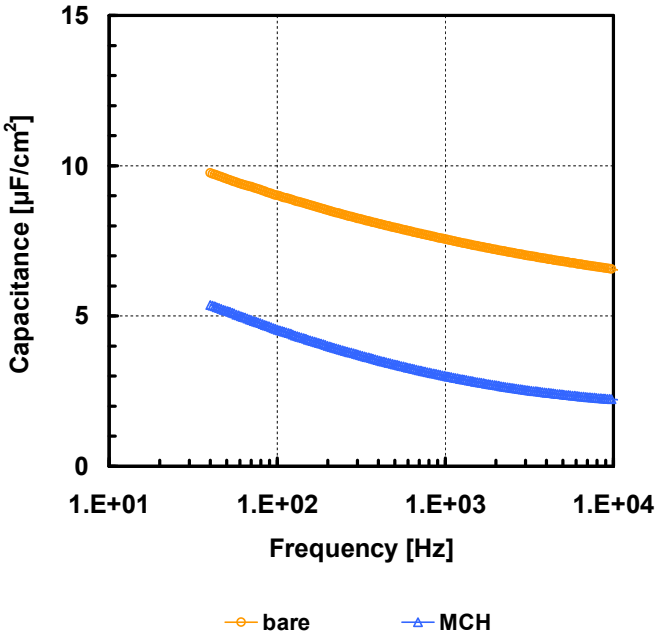

(a)

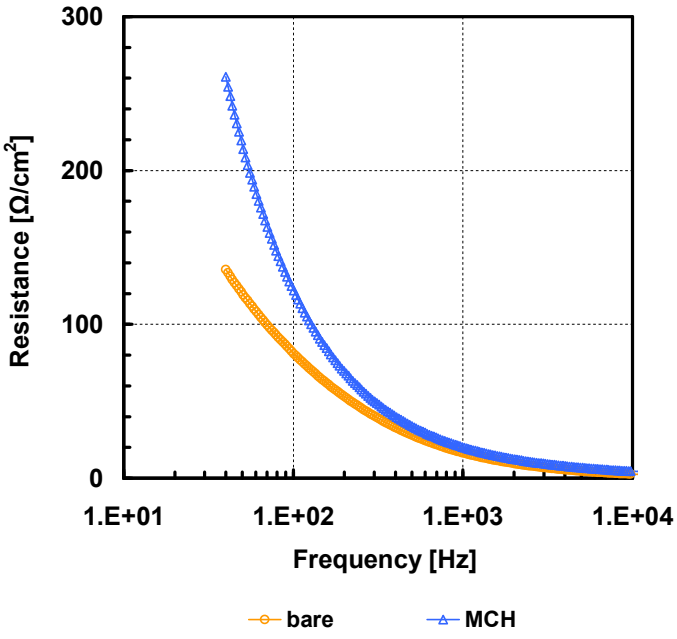

(b)

Fig. 4.11 Frequency dependence of (a) interfacial capacitance and (b) interfacial resistance.

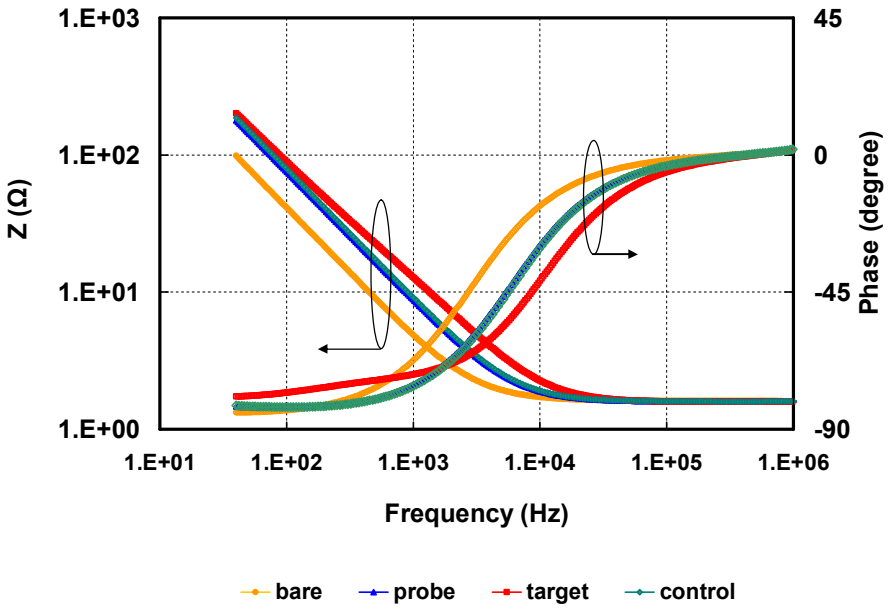

Fig. 4.12 Bode plots of bare electrode (bare), probe immobilization (probe), target hybridization (target), and electrode after noncomplementary binding (control).

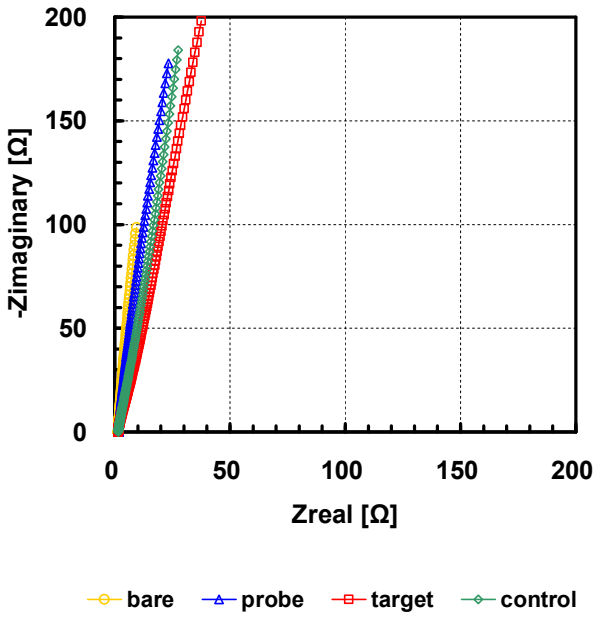

Fig. 4.13 Nyquist plots of bare electrode, probe immobilization, target hybridization, and electrode after noncomplementary binding.

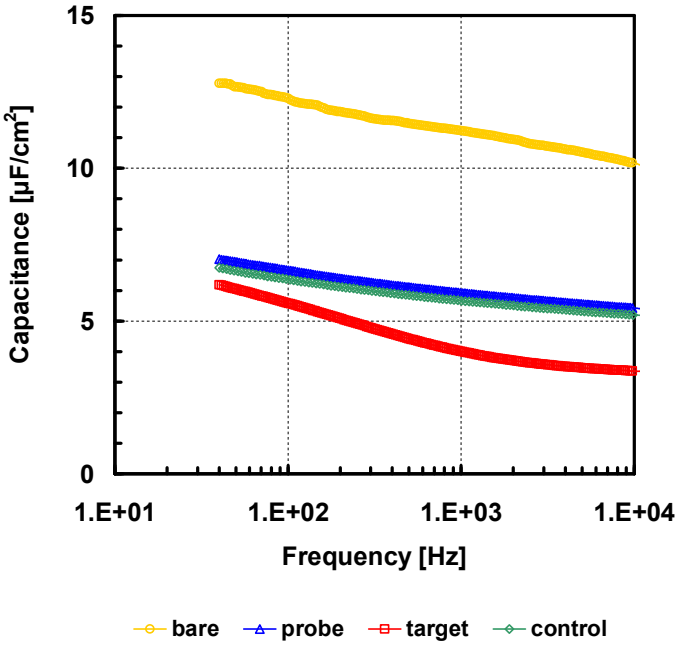

(a)

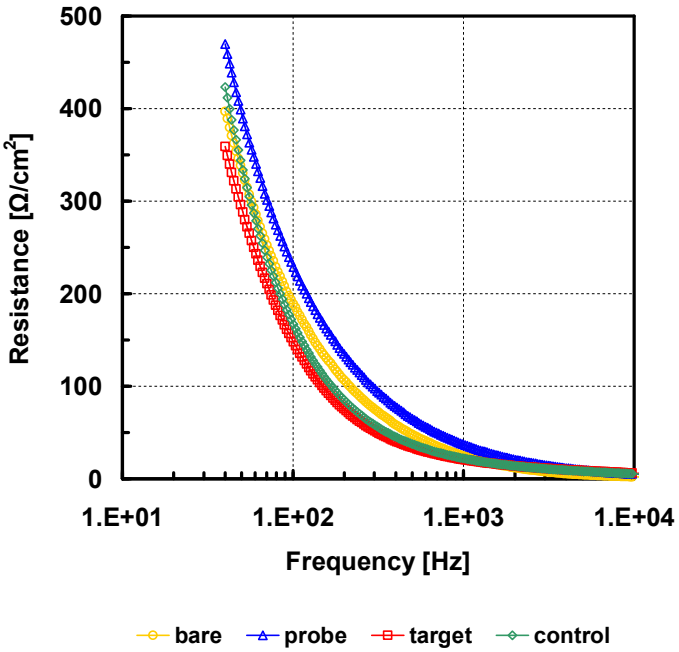

(b)

Fig. 4.14 Interfacial (a) capacitance and (b) resistance as a function of frequency at DNA measurement using probe immobilized electrode.

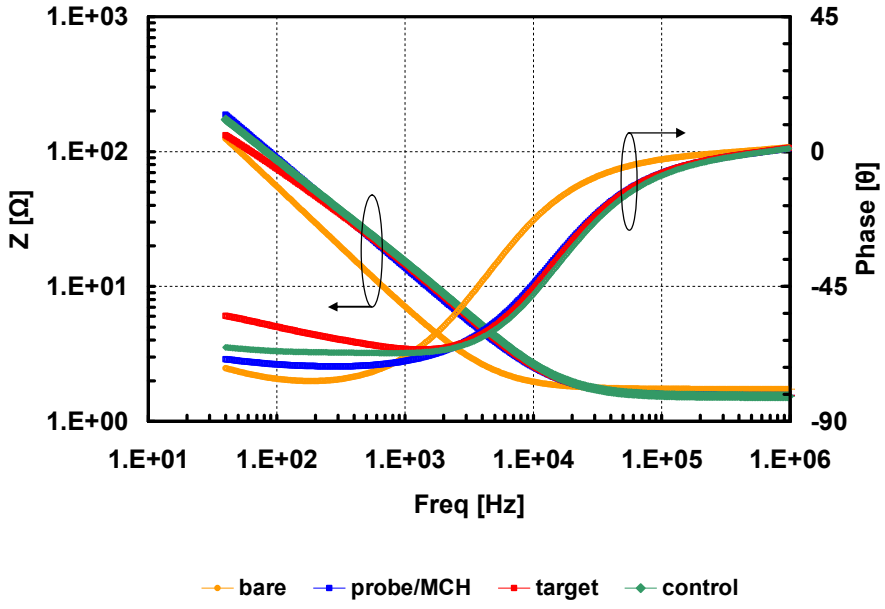

Fig. 4.15 Bode plots of bare electrode (bare), probe immobilization with MCH-backfilled (probe/MCH), target hybridization (target), and electrode after noncomplementary binding (control).

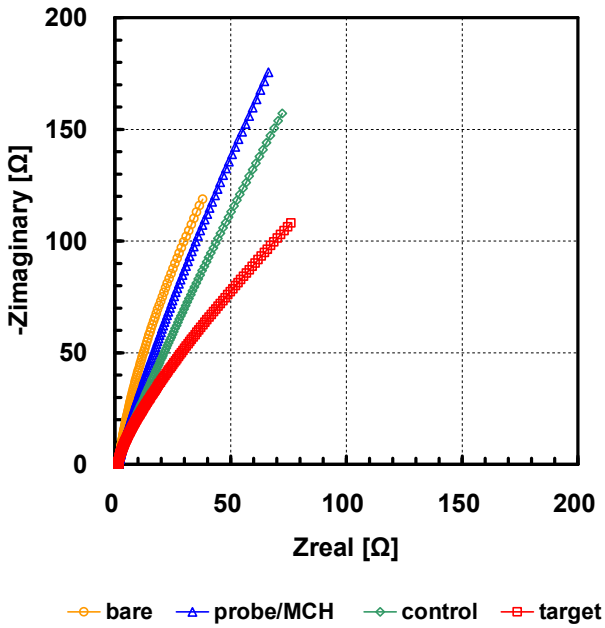

Fig. 4.16 Nyquist plots of bare electrode, probe/MCH immobilization, target hybridization, and electrode after noncomplementary binding.

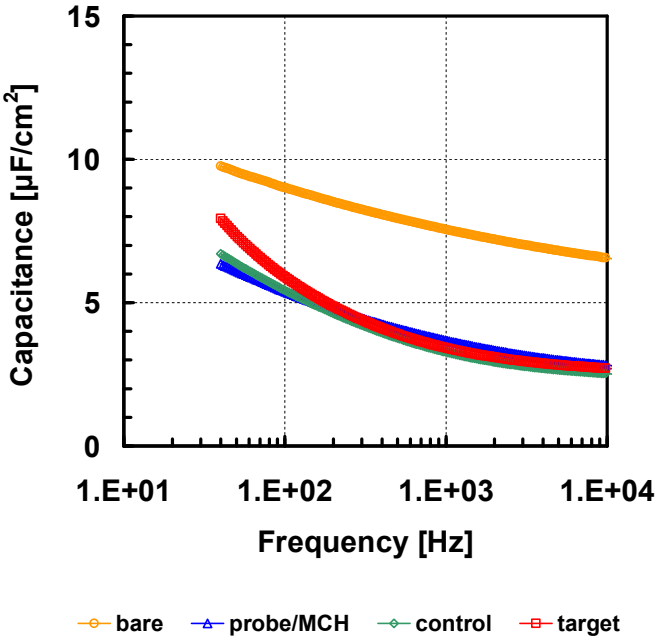

(a)

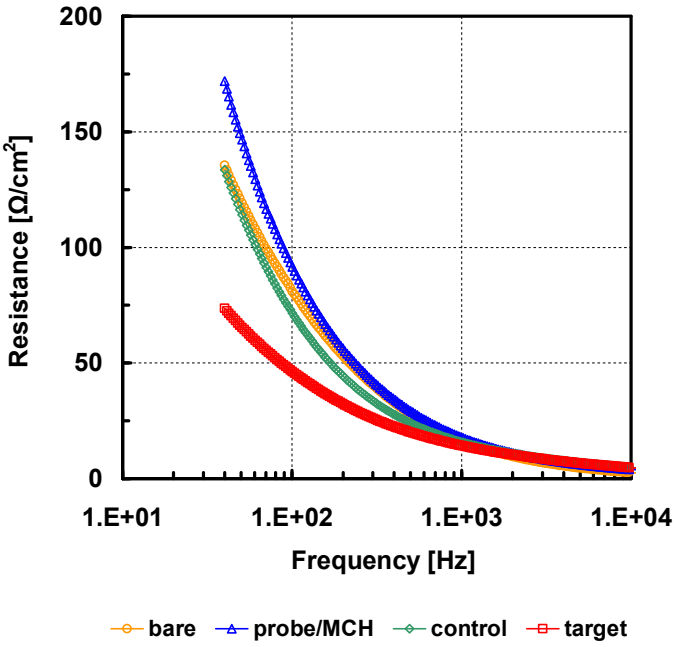

(b)

Fig. 4.17 Interfacial (a) capacitance and (b) resistance as a function of frequency at DNA measurement using probe/MCH immobilized electrode.

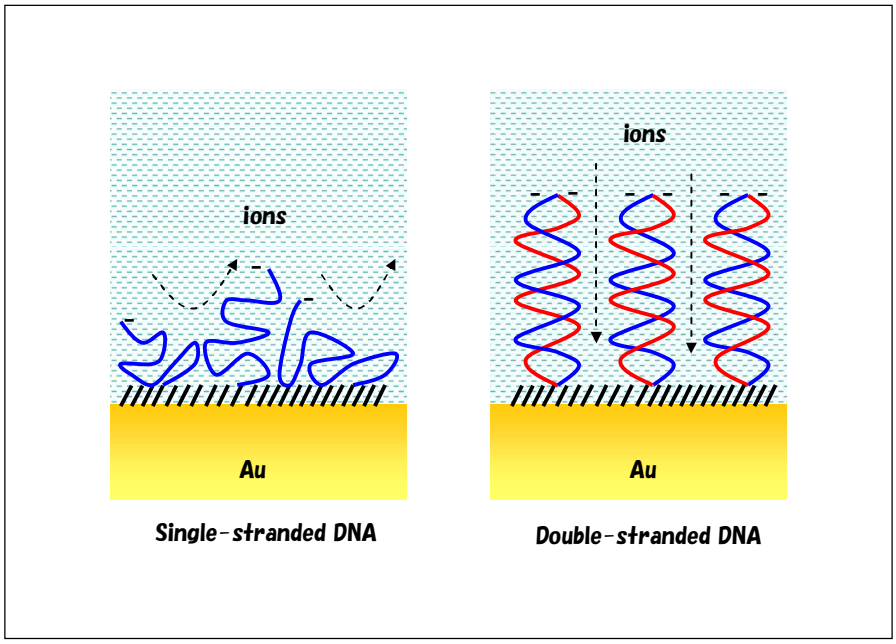

Fig. 4.18 Illustration of DNA physical changes upon DNA hybridization.

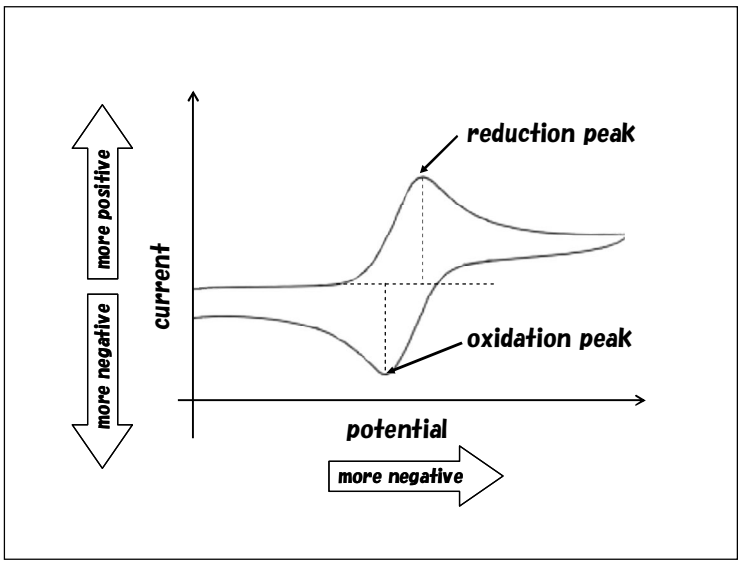

Fig. 4.19 Typical cyclic voltammogram.

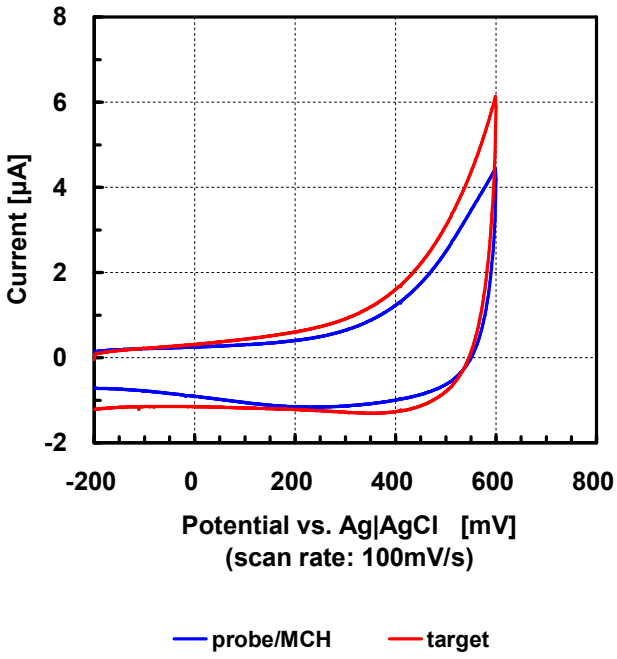

Fig. 4.20 Cyclic voltammograms of electrode after probe attachment followed by MCH-backfilled (probe/MCH) and electrode after complementary binding (target).

Chapter 5

Conclusions

This thesis work is inserted in the field of nonfaradaic impedimetric biosensor, particularly for detection of specific DNA hybridization. Considering the advantages of single chip integration for rapid, low cost and portable point-of-care device, we are motivated to develop a fully label-free, integrated capacitance biosensor for DNA diagnostic applications. An on-chip microelectrode biosensor combined with CMOS readout circuitry is proposed. Detection of DNA hybridization is demonstrated using the fabricated chip based on current available CMOS technology. The result shows that hybridization can be detected by monitoring the double layer capacitance variation before and after target DNA exposure. Compared to available literatures (at least to the best of our knowledge), it is believed that this work is in advance in terms of a single chip detection, fully differential approach at sensing/measurement circuit and wide frequency detection of DNA hybridization. Problems related to reliable and sensitive measurements are still open since on-chip detection reported in this thesis is performed by assumption that based on others published works (i.e. capacitance decrease upon DNA hybridization). We took the initiative to develop a system for investigation of biochemical phenomenon underlying the capacitance variation. Electrochemical impedance spectroscopy (EIS) is used to study the electrode surface reactions introduced by DNA hybridization. It is shown that the impedance (or capacitance) change may due to the physical changes of DNA molecules and the surface preparation plays an important role in capacitance-based biosensor performance. It is hoped that our findings would provide a better understanding on the associated impedance changes caused by DNA hybridization and help in guiding the development of a sensitive yet reliable DNA biosensor. With the creativity of scientists and advances in technology involved, there is no doubt that in the near future, electrical biosensors will become a powerful tool for genomic assays at point-of-care environment.

Chapter 6

Future works

The feasibility of a nonfaradaic impedimetric sensing for DNA detection has been explored in Chapter 3 and 4. This chapter presents ongoing works towards array integration of capacitance sensor and improvement in detection method for more sensitive and reliable DNA measurement.

6.1 Capacitance sensor array

In Chapter 3 it was shown that the capacitive method exploiting double layer characteristics can be used to perform on-chip biosensing. The application of our device can be extended beyond DNA detection to other biomolecules, including cells, proteins, and antigens as they have their unique impedance value. As high throughput analysis is desirable for rapid diagnosis, the integration of a large number of sensor units onto a single chip is vital. In this section, the possibility of the proposed sensor towards array implementation is described.

The array structure is illustrated in Fig. 6.1. Only the CBCM front-end is put into the matrix, whereas the back-end current-to-voltage conversion (IVC) circuit (consisting of a switched-capacitor integrator and operational amplifier) is shared between the matrix cells of each column. The column-parallel architecture gives advantage in terms of layout matching as symmetrical design is very important in differentially circuitry we adopted here. An array-clock controller (ACC) unit is designed to selectively activate the array cell. Two array clock pulses, a_{CN} and a_{CP}, for complimentary switches in CBCM cell are simply generated when the gate-control signal, V_G is in a high state; otherwise, the MOSFETs will be switched off. Mutual existence of the proposed ACC and CBCM in a matrix gives tradeoffs between performance and area, where the control scheme to activate only one cell at a time could reduce power consumption and overcome the crosstalk problem, but would cost an increase in array footprint.

When a multiple number of matrix cells are arranged in a matrix, a large parasitic capacitance is expected to exist at the input nodes of the shared IVC unit. To prevent degradation of IVC

performance, an operational amplifier with sufficiently high gain is required. A differential double-ended operational amplifier based on folded cascade configuration is proposed (Fig. 6.2). The common-mode voltage is held at a reference voltage V_{CM} and the feedback is achieved by controlling the bias voltage of tail-current transistor M_9. Self-biasing circuit to generate reference voltages V_{b1}, V_{b2}, and V_{b3} for the amplifier is carefully designed to have low dependence on device parameter and temperature variations. Circuit optimization is done based on 1.2 μm CMOS technology. A maximum gain of 75 dB and phase margin of about 77° is achieved (Fig. 6.3). At array implementation, the common-mode feedback and self-biasing circuits (CMFB/SB) is shared between the column-parallel IVC units. Simulated result of 4 × 4 array is shown in Fig. 6.4.

The circuit layout using 1.2 μm, 2-metal, 2-poly CMOS technology is shown in Fig. 6.5 and the area of the array is 450 μm × 300 μm. The chip fabrication is now under way.

6.2 Integrated impedance biosensor

As discussed in Chapter 4, the impedance change at electrode-solution interface is affected both by the resistance and capacitance. A new approach that can provide a more stable measurement of DNA detection is desirable. The development of an impedance-based biosensor is now at the early stage. CMOS detection circuit is designed so that it is able to detect a variation in the absolute impedance (combination of resistance and capacitance) of the electrode-solution interface. The schematic of the proposed circuit is shown in Fig. 6.6. The purpose of this circuit is to fix the electrode voltage and measure ac current, reducing the parasitic capacitance effect. The circuit is simulated using SPICE for various value of R_S at |Vi|=0.1 V, I_{SS}=10μA, C_d=10^{-12} F, and C_p=10^{-13} F. It is shown in Fig. 6.7 that the proposed circuit is able to detect the variation of impedance change as two peaks of current can be observed. There is a hope that this new sensor can be establish in the near future and provide improvement in terms of sensitivity and reliability towards biomolecules detection, particularly DNA hybridization.

6.3 Figures

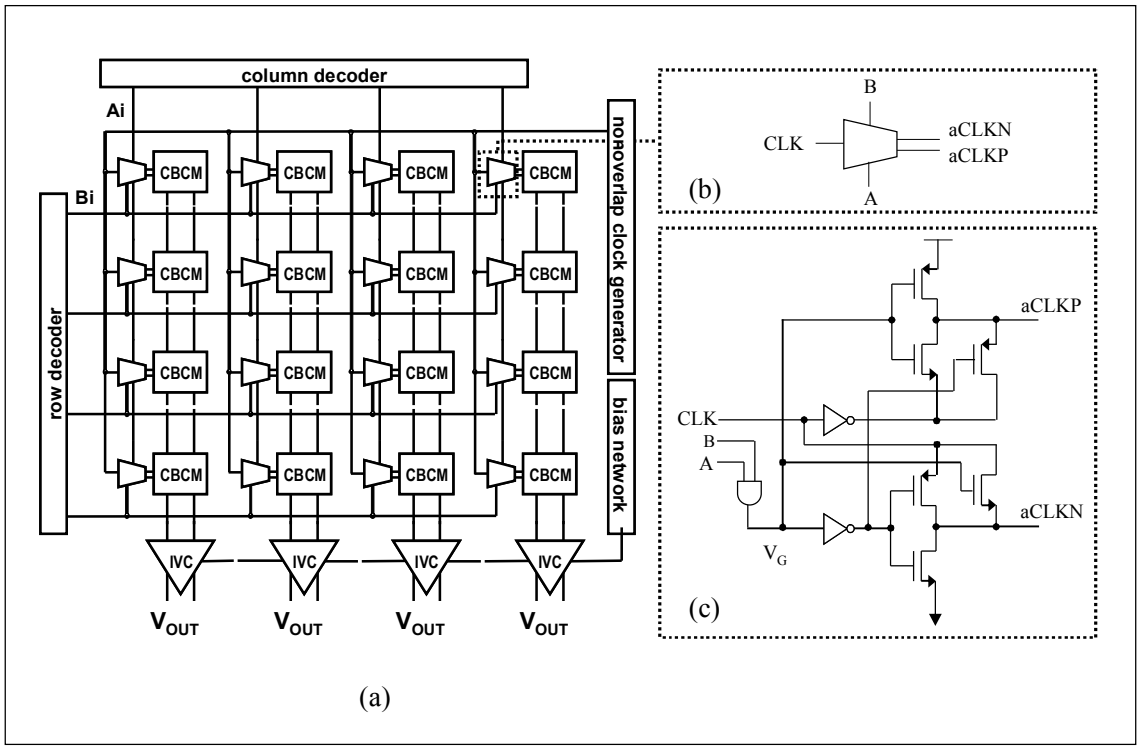

Fig. 6.1 (a) Fully differential sensor array with (b) array clock controller, and (c) its schematic.

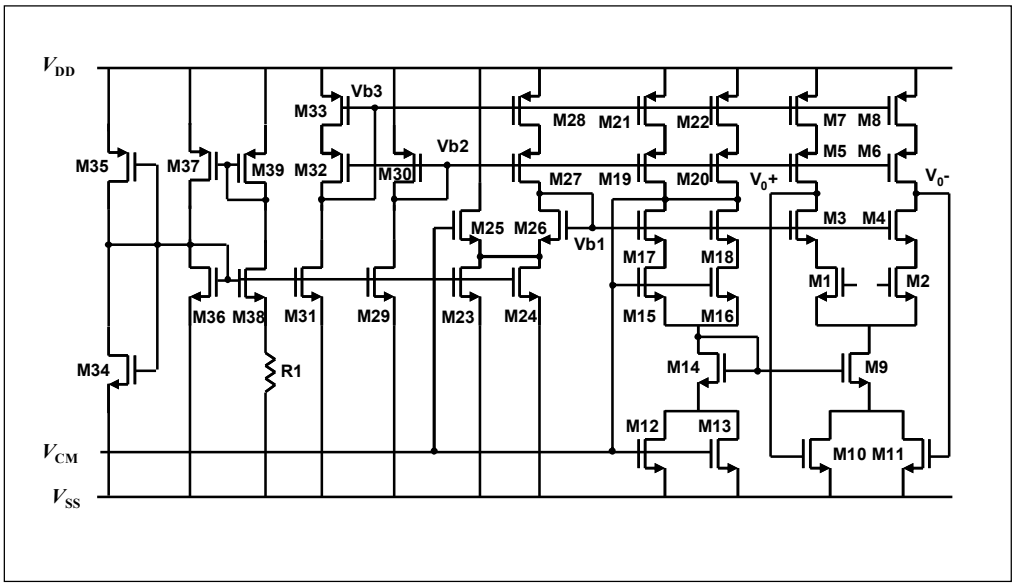

Fig. 6.2 Transistor-level of differential operational amplifier.

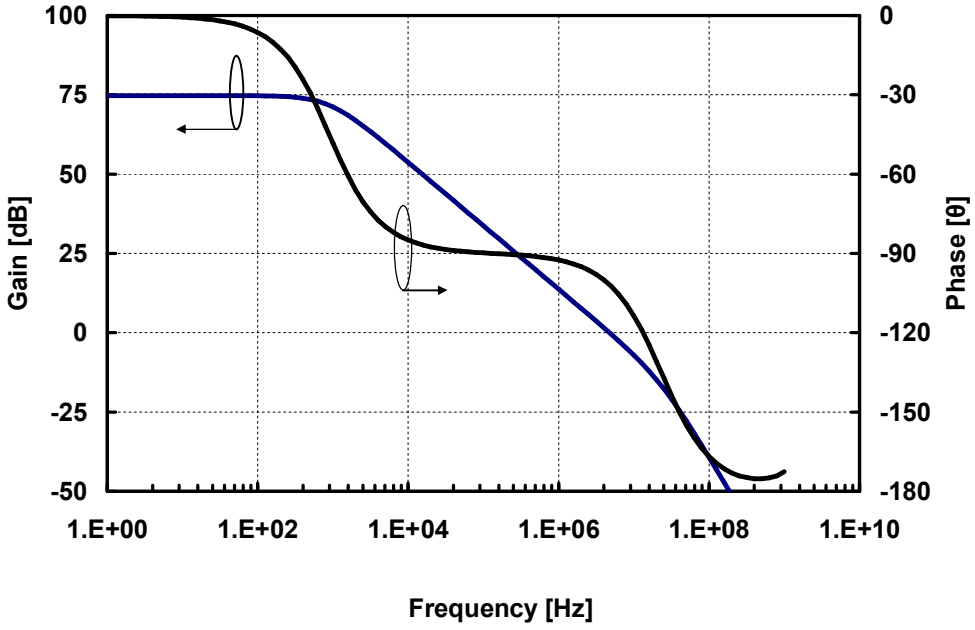

Fig. 6.3 Gain and phase characteristics of the operational amplifier.

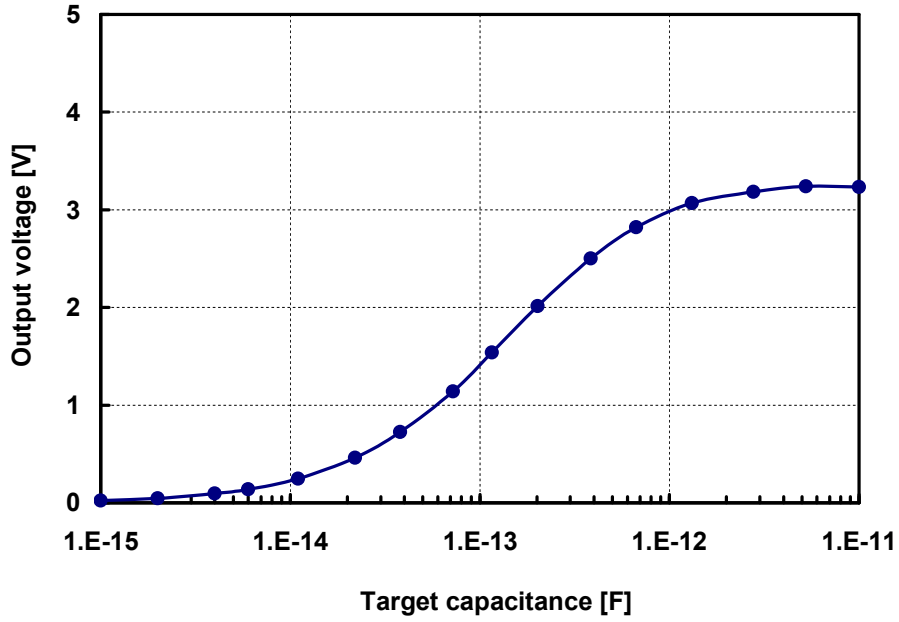

Fig. 6.4 Simulated result of 4×4 array with different values of input capacitances are placed at each cell.

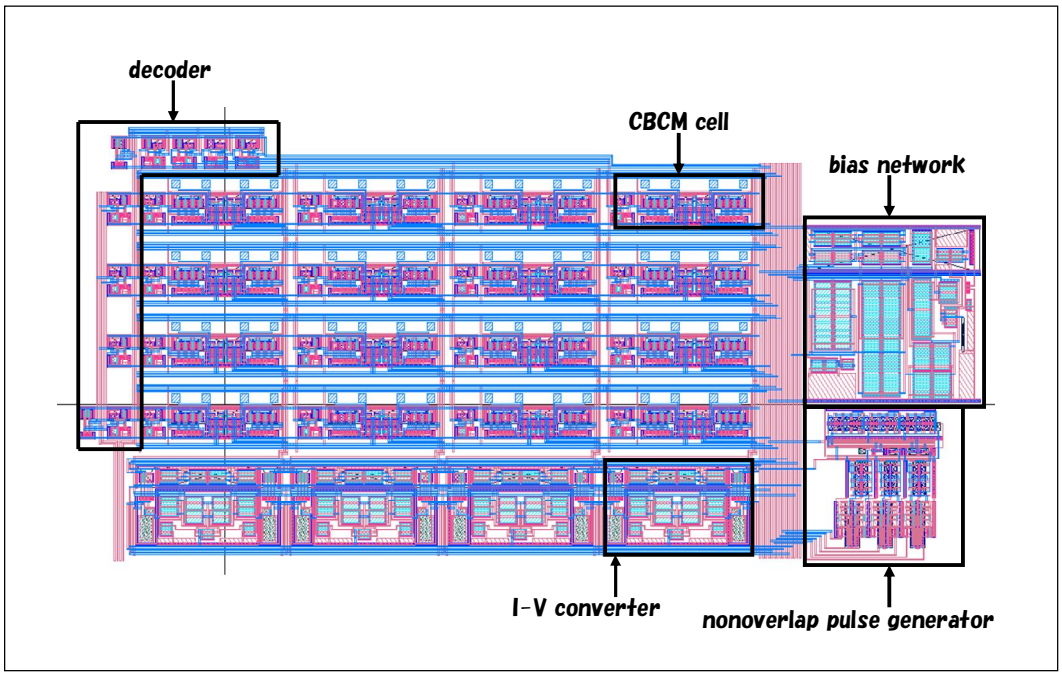

Fig. 6.5 Layout of 4 × 4 array featuring column-parallel current-to-voltage converter with bias network and nonoverlap pulse generator.

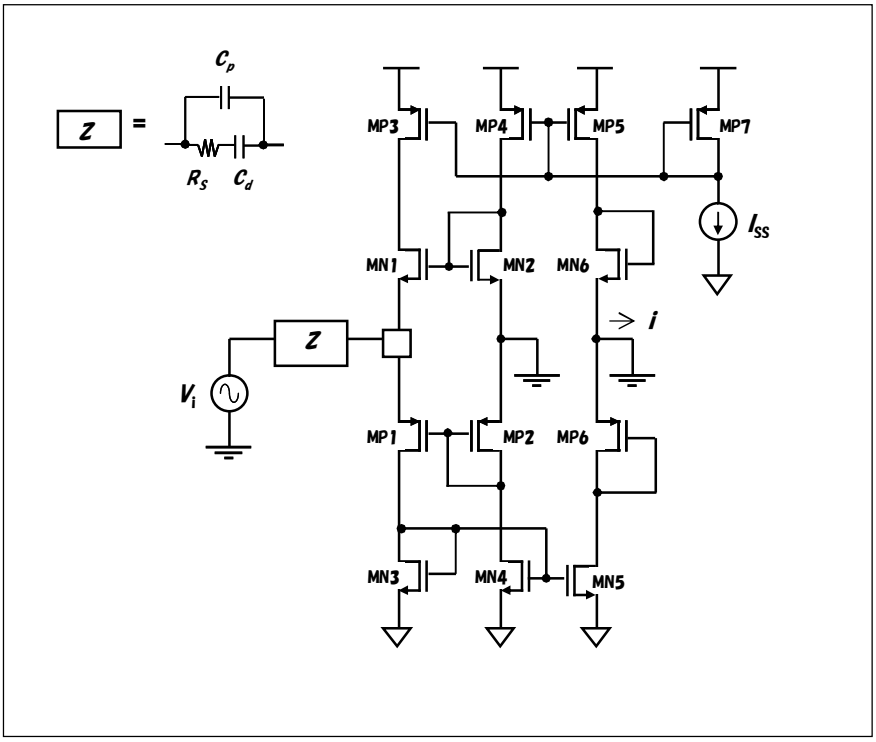

Fig. 6.6 A proposed impedance biosensor circuit.

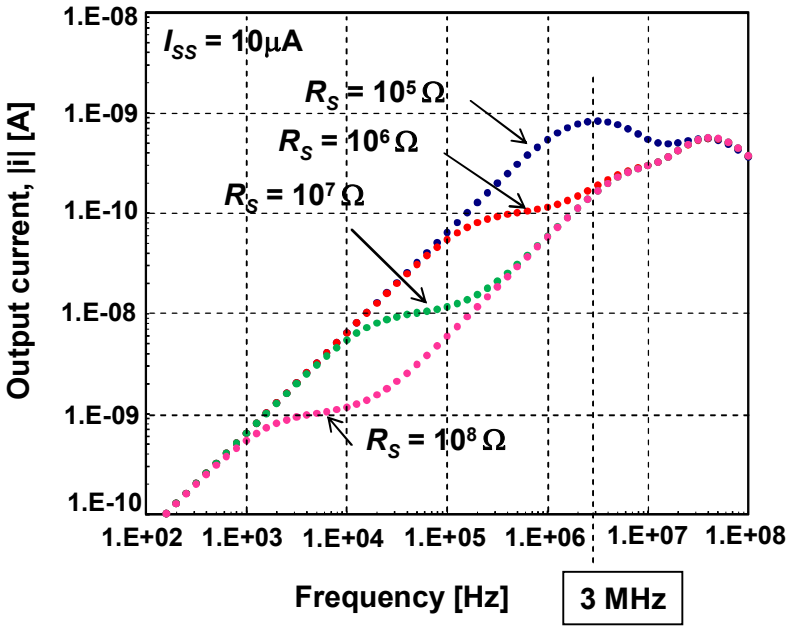

Fig. 6.7 Simulated result of the proposed impedance biosensor.

List of figures

List of tables

Curriculum vitae

Yusmeeraz Binti Yusof

Department of Electrical Engineering and Computer Science, Graduate School of Engineering, Nagoya University, Furo-cho, Chikusa-ku, Nagoya 464-8603, Japan.

Phone: (052) 789 3307 Email: b_yusof@nuee.nagoya-u.ac.jp, yusmeeraz.yusof@gmail.com

Education

1998-2002 BSc in Electronics and Electrical Engineering, Keio University, Tokyo, Japan

2002-2004 MSc in Integrated Design Engineering, Keio University, Tokyo, Japan

2008-2011 Doctoral course in Engineering, Nagoya University, Nagoya, Japan

Work experience

2004-2005 Alps Electric (Malaysia) Sdn. Bhd., Negeri Sembilan, Malaysia

2006~present Universiti Teknologi Malaysia, Johor, Malaysia (on study leave 2008-2011)

List of publications

Journal paper

1. Y. Yusof, K. Sugimoto, H. Ozawa, S. Uno, K. Nakazato, *On-chip Microelectrode Capacitance Measurement for Biosensing Applications.* Jap. J. Appl. Phys., 2010, Vol. 49, pp. 01AG05-1-6.
2. Y. Yusof, Y. Yanagimoto, S. Uno, K. Nakazato, *Electrical characteristics of biomodified electrodes using nonfaradaic electrochemical impedance spectroscopy.* World Acad. Sci. Eng. Technol., 2011, Vol. 73, pp. 295-299.

International Conference

1. K. Sugimoto, Y. Yusof, H. Ozawa, S. Uno, K. Nakazato, *Capacitance Sensor Array based on Charge Based Capacitance Measurement for DNA Detection.* 5th International Conference on Molecular Electronics and Bioelectronics, 2009.
2. Y. Yusof, Y. Yanagimoto, S. Uno, K. Nakazato, *Electrical characteristics of biomodified electrodes using nonfaradaic electrochemical impedance spectroscopy.* International Conference on Bioinformatics and Biomedical Engineering, 2011.